Engineering with Computers
https://doi.org/10.1007/s00366-025-02182-4

ORIGINAL ARTICLE

Polytopal discontinuous Galerkin methods for low-frequency poroelasticity coupled to unsteady Stokes flow

Michele Botti[1] · **Ivan Fumagalli**[1] · **Ilario Mazzieri**[1]

Received: 31 January 2025 / Accepted: 10 July 2025
© The Author(s) 2025

Abstract
We focus on the numerical analysis of a polygonal discontinuous Galerkin scheme for the simulation of the exchange of fluid between a deformable saturated poroelastic structure and an adjacent free-flow channel. We specifically address wave phenomena described by the low-frequency Biot model in the poroelastic region and unsteady Stokes flow in the open channel, possibly an isolated cavity or a connected fracture system. The coupling at the interface between the two regions is realized by means of transmission conditions expressing conservation laws. The spatial discretization hinges on the weak form of the two-displacement poroelasticity system and a stress formulation of the Stokes equation with weakly imposed symmetry. We present a complete stability analysis for the proposed semi-discrete formulation and derive a-priori hp-error estimates.

Keywords Multiphysics · Polygonal and polyhedral meshes · Stability and convergence analysis · Wave propagation

Mathematics Subject Classification Primary 65M12 · 65M60

1 Introduction

This paper presents a new discontinuous Galerkin formulation for the numerical solution of the dynamic Stokes–Biot problem, which models the interaction between the free flow of an incompressible fluid and a deformable porous medium. This coupled phenomenon, known as fluid-poroelastic structure interaction, has gained significant attention in recent years due to its wide range of applications, including geomechanical modeling, hydrogeology, environmental science, and biomedical engineering: see, e.g., [1–6]. Specific examples include predicting and managing gas and oil extraction processes from fractured reservoirs [7], groundwater flow cleanup in deformable aquifers [8], industrial filter design [9], and modeling blood-vessel interactions in blood flow [10, 11]. Such problems can be modeled through the unsteady Stokes equations, governing the fluid dynamics, and the low-frequency poroelasticity system, describing the wave propagation in the deformable saturated porous medium [12]. The Stokes and Biot regions are coupled through transmission conditions at the interface that enforce the continuity of normal flux, the Beavers-Joseph-Saffman (BJS) slip condition with friction for the tangential velocity, the stress balance, and the continuity of normal stress, cf. [13].

The first mathematical analysis of the Stokes–Biot system reformulated as a parabolic system appeared in [12], while the well-posedness for the fully dynamic Navier–Stokes/Biot system, using a pressure-based Darcy formulation, was established in [14]. The coupling of the Stokes–Biot system with transport processes was analysed in [15], while a dimensionally reduced Brinkman–Biot model for fracture flow in poroelastic media was developed and analyzed in [16].

Michele Botti, Ivan Fumagalli and Ilario Mazzieri contributed equally to this work.

✉ Ilario Mazzieri
ilario.mazzieri@polimi.it

Michele Botti
michele.botti@polimi.it

Ivan Fumagalli
ivan.fumagalli@polimi.it

[1] MOX-Laboratory for Modeling and Scientific Computing, Department of Mathematics, Politecnico di Milano, P.za Leonardo da Vinci, 32, Milan 20133, Italy

Published online: 13 August 2025

In recent years, a variety of discretization techniques have been introduced for the Stokes–Biot system, including mixed finite element methods [17, 18], a staggered finite element method [19], and a non-conforming finite element method [20]. Also in terms of coupling strategies and algorithms, several approaches have been proposed in the literature. The work in [21] employed Nitsche's method to weakly enforce the continuity of normal flux, while [22] introduced a Lagrange multiplier formulation for imposing this continuity. In [23], a non-iterative operator splitting scheme was introduced for an arterial flow model featuring a thin elastic membrane between two regions, utilizing a pressure-based formulation for flow in the poroelastic domain. In [24], a second-order decoupling scheme was proposed for a nonlinear Stokes–Biot model. The numerical investigation presented in [25] offered both monolithic and iterative partitioned solutions, addressing at the same time the fluid-poroelasticity coupling and the flow complexity associated to the Navier–Stokes equations and to the subgrid scales modeled in a variational multiscale frame.

In this paper, we consider the following formulation of the Biot–Stokes system. In the poroelastic domain, we address wave propagation using the low-frequency Biot model written in the so-called two-displacement formulation [26]. On the other hand, in the fluid domain, we consider the stress formulation of the Stokes equation, similar to [27], with weakly-imposed symmetry. This choice is suggested by the transmission conditions at the interface between the two domains, expressing conservation laws in terms of relations between stress and flow. In particular, this strategy allows us to avoid both the introduction of a Lagrange multiplier unknown to enforce the coupling as done, e.g., in [22], and additional penalty terms at the interface as in [28]. We discretize in space the resulting system of equations utilizing a polygonal discontinuous Galerkin scheme (PolydG), [29]. The PolydG method provides several advantages for addressing coupled problems. These include: (i) the capability to accurately represent complex geometries, (ii) a natural framework for mesh refinement and agglomeration strategies, (iii) the effective handling of non-conforming interfaces, (iv) robustness in the presence of heterogeneous physical properties, and (v) support for arbitrary polynomial approximation orders. Additionally, its geometric flexibility facilitates the efficient enforcement of transmission conditions, which are often confined to specific subregions of the computational domain, without sacrificing computational efficiency. PolydG discretizations have been applied successfully to several studies addressing different classes of differential problems such as: second-order elliptic problems [29] - and references therein -, parabolic differential equations [30], flows in fractured porous media [31], fluid–structure interaction problems [32], elastodynamics [33], nonlinear sound waves [34], coupled wave propagation problems [26, 28, 35–37], thermo-elasticity [38, 39], and multi-physics brain modeling [40–43].

The goal of this paper is to propose for the first time a discontinuous Galerkin method—in particular, a PolydG method— for the Biot–Stokes system in the aforementioned formulation. Since this formulation of the coupled problem is new in the literature, we present a stability analysis at the continuous level. Then, we derive stability and error estimates for the semidiscrete problem. Regarding the latter, we rely on an extension of an inf-sup inequality that holds for a discretization of the linear elasticity equations based on conforming simplicial meshes [44]. We extend this result to our dG method in the case of simplicial meshes and then assume it is also valid for polygonal meshes. The proof of this assumption will be the subject of future work; nevertheless, the numerical tests presented in this paper confirm our theoretical results.

We organize the rest of the paper as follows. In Sect. 2 we present the mathematical model, which includes the derivation of the stress formulation of the Stokes problem and the continuous weak formulation. The spatial discretization with the PolydG method is addressed in Sect. 3, as well as the stability and error analysis for the semidiscrete problem. Time integration and numerical experiments are presented in Sects. 4 and 5, respectively. Finally, in Sect. 6 we draw some conclusions.

2 The physical model and governing equations

We introduce the dynamic poroelasticity model, the unsteady Stokes problem, and the transmission conditions describing the interaction between the two systems. Then, we derive the variational formulation of the coupled problem and investigate its well-posedness. We start this section by introducing some instrumental notation.

2.1 Notation

Let $\Omega \subset \mathbb{R}^d$, $d = 2, 3$ be an open, convex polytopal domain decomposed as the union of two disjoint, polytopal subdomains, i.e., Ω is the interior part of $\bar{\Omega}_p \cup \bar{\Omega}_f$, representing the poroelastic and the fluid domains, respectively. The two subdomains share part of their boundary, resulting in the interface $\Gamma_I = \partial\Omega_p \cap \partial\Omega_f$. The Lipschitz boundary of Ω is denoted by $\partial\Omega = \Gamma_p \cup \Gamma_f$, where $\Gamma_\diamond = \partial\Omega_\diamond \setminus \Gamma_I$, for $\diamond = \{p, f\}$, being $\partial\Omega_\diamond$ the union of two disjoint portions $\Gamma_\diamond^D$ and $\Gamma_\diamond^N$ with positive $(d-1)$-dimensional measure and where Dirichlet and Neumann conditions are imposed, respectively. The outer unit normal vectors to $\partial\Omega_p$ and $\partial\Omega_f$

are denoted by $\boldsymbol{n}_p$ and $\boldsymbol{n}_f$, respectively, so that $\boldsymbol{n}_f = -\boldsymbol{n}_p$ on Γ_I.

In the following, for a simply connected $X \subset \Omega$ and $\ell \geq 0$, the notation $\boldsymbol{H}^\ell(X)$ will be employed in place of $[H^\ell(X)]^d$ for vector valued Sobolev spaces, assuming by convention that $\boldsymbol{H}^0(X) \equiv \boldsymbol{L}^2(X)$. Moreover, we will denote with $(\cdot,\cdot)_X$ the scalar product in $\boldsymbol{L}^2(X)$ and with $||\cdot||_X$ the associated norm. In addition, we will use $\boldsymbol{H}(\mathrm{div}, X)$ to denote the space of $\boldsymbol{L}^2(X)$ functions with square integrable divergence. A similar notation will be adopted for tensor-valued functions, i.e. $\mathbb{L}^2(X)$ and $\mathbb{H}(\mathrm{div}, X)$ stand for $[\boldsymbol{L}^2(X)]^{d\times d}$ and $[\boldsymbol{H}(\mathrm{div}, X)]^{d\times d}$, respectively. In order to take into account essential boundary conditions, we also introduce the zero-trace subspaces, defined as

$$\begin{aligned}
\boldsymbol{H}^1_{0,\Gamma_p^D}(\Omega_p) &= \{\boldsymbol{v} \in \boldsymbol{H}^1(\Omega_p) \,|\, \boldsymbol{v}_{|\Gamma_p^D} = \boldsymbol{0}\},\\
\boldsymbol{H}_{0,\Gamma_p^D}(\mathrm{div}, \Omega_p) &= \{\boldsymbol{z} \in \boldsymbol{H}(\mathrm{div}, \Omega_p) \,|\, (\boldsymbol{z}\cdot\boldsymbol{n}_p)_{|\Gamma_p^D} = 0\},\\
\mathbb{H}_{0,\Gamma_f^N}(\mathrm{div}, \Omega_f) &= \{\boldsymbol{\tau} \in \mathbb{H}(\mathrm{div}, \Omega_f) \,|\, (\boldsymbol{\tau}\boldsymbol{n}_f)_{|\Gamma_f^N} = \boldsymbol{0}\}.
\end{aligned}$$

For a given final time $T > 0$, $k \in \mathbb{N}$, and a Hilbert space H, the usual notation $C^k([0,T]; H)$ is adopted for the space of H-valued functions, k-times continuously differentiable in $[0, T]$. The notation $x \lesssim y$ stands for $x \leq Cy$, with $C > 0$ independent of the discretization parameters, but possibly dependent on the physical coefficients and the final time T.

In the following, for tensor fields $\boldsymbol{\tau}$ we will use the notation

$$\mathrm{tr}(\boldsymbol{\tau}) = \sum_{i=1}^{d} \tau_{ii}, \quad \mathrm{dev}(\boldsymbol{\tau}) = \boldsymbol{\tau} - \frac{1}{d}\mathrm{tr}(\boldsymbol{\tau})\boldsymbol{I}, \quad \mathrm{skew}(\boldsymbol{\tau}) = \frac{\boldsymbol{\tau} - \boldsymbol{\tau}^{\mathrm{T}}}{2},$$

to indicate the trace, the deviatoric part, and the skew symmetric part of $\boldsymbol{\tau}$, respectively.

2.2 The poroelasto-fluid problem

In the poroelastic domain Ω_p, for a final observation time $T > 0$, we consider the following Biot equations, cf. [45, 46]:

$$\begin{cases}
\rho\ddot{\boldsymbol{u}}_p + \rho_f\ddot{\boldsymbol{w}}_p - \nabla\cdot\boldsymbol{\sigma}_p = \boldsymbol{f}_p, & in\ \Omega_p\times(0,T],\\
\rho_f\ddot{\boldsymbol{u}}_p + \rho_w\ddot{\boldsymbol{w}}_p + \frac{\eta}{\kappa}\dot{\boldsymbol{w}}_p + \nabla p_p = \boldsymbol{g}_p, & in\ \Omega_p\times(0,T],\\
\boldsymbol{u}_p = \boldsymbol{0}, & on\ \Gamma_p^D\times(0,T],\\
\boldsymbol{w}_p\cdot\boldsymbol{n}_p = 0, & on\ \Gamma_p^D\times(0,T],\\
\boldsymbol{\sigma}_p\boldsymbol{n}_p = \boldsymbol{g}_p^N, & on\ \Gamma_p^N\times(0,T],\\
p_p = q_p^N, & on\ \Gamma_p^N\times(0,T],\\
\boldsymbol{u}_p = \boldsymbol{u}_{p0}, \quad \dot{\boldsymbol{u}}_p = \boldsymbol{v}_{p0}, & in\ \Omega_p\times\{0\},\\
\boldsymbol{w}_p = \boldsymbol{w}_{p0}, \quad \dot{\boldsymbol{w}}_p = \boldsymbol{z}_{p0}, & in\ \Omega_p\times\{0\},
\end{cases} \tag{1}$$

where $\boldsymbol{u}_p$ is the solid and $\boldsymbol{w}_p$ is the filtration displacement, respectively. In (1), the average density ρ is given by $\rho = \phi\rho_f + (1-\phi)\rho_s$, where $\rho_s > 0$ is the solid density, $\rho_f > 0$ is the saturating fluid density, and ρ_w is defined as $\rho_w = \frac{a}{\phi}\rho_f$, with ϕ being the porosity satisfying $0 < \phi_0 \leq \phi \leq \phi_1 < 1$ and $a \geq 1$ the tortuosity measuring the deviation of the fluid paths from straight streamlines. In (1), $\eta > 0$ represents the dynamic viscosity of the fluid, $k > 0$ is the absolute permeability, $\boldsymbol{f}_p, \boldsymbol{g}_p, \boldsymbol{g}_p^D$ and q_p^N are given (regular enough) loading and source terms, respectively, and $\boldsymbol{u}_{p0}, \boldsymbol{v}_{p0}, \boldsymbol{w}_{p0}$, and $\boldsymbol{z}_{p0}$ are regular enough given initial conditions. In Ω_p, we assume the following constitutive laws which allow to express the pore pressure p_p and stress tensor $\boldsymbol{\sigma}_p$ in terms of the two displacements $\boldsymbol{u}$ and $\boldsymbol{w}$:

$$p_p(\boldsymbol{u},\boldsymbol{w}) = -m(\beta\nabla\cdot\boldsymbol{u} + \nabla\cdot\boldsymbol{w}), \qquad \boldsymbol{\sigma}_p(\boldsymbol{u},\boldsymbol{w}) = \boldsymbol{\sigma}_e(\boldsymbol{u}) - \beta p_p(\boldsymbol{u},\boldsymbol{w})\boldsymbol{I}, \tag{2}$$

where the elastic stress $\boldsymbol{\sigma}_e(\boldsymbol{u}) = \mathbb{C}\boldsymbol{\varepsilon}(\boldsymbol{u}) = 2\mu\boldsymbol{\varepsilon}(\boldsymbol{u}) + \lambda(\nabla\cdot\boldsymbol{u})\boldsymbol{I}$, being $\mathbb{C}$ the stiffness tensor and $\boldsymbol{\varepsilon}(\boldsymbol{u}) = \frac{1}{2}(\nabla\boldsymbol{u} + \nabla\boldsymbol{u}^T)$ the strain tensor (symmetric gradient). In (2), $\lambda \geq 0$ and $\mu \geq \mu_0 > 0$ are the Lamé coefficients of the elastic skeleton. The Biot–Willis coefficient β and Biot modulus m are such that $\phi < \beta \leq 1$ and $m \geq m_0 > 0$.

In the fluid domain Ω_f, we consider a free incompressible viscous fluid with mass density $\rho_f > 0$ and dynamic viscosity $\mu_f > 0$. Assuming that the fluid viscosity is sufficiently high, the Stokes' system of equations governs the fluid flow:

$$\begin{cases}
\dot{\boldsymbol{u}}_f - \rho_f^{-1}\nabla\cdot\boldsymbol{\sigma}_f = \boldsymbol{h}_f, & in\ \Omega_f\times(0,T],\\
\nabla\cdot\boldsymbol{u}_f = 0, & in\ \Omega_f\times(0,T],\\
\boldsymbol{u}_f = \boldsymbol{g}_f^D, & on\ \Gamma_f^D,\times(0,T],\\
\boldsymbol{\sigma}_f\boldsymbol{n}_f = \boldsymbol{g}_f^N, & on\ \Gamma_f^N\times(0,T],\\
\boldsymbol{u}_f = \boldsymbol{u}_{f0}, & in\ \Omega_f\times\{0\},
\end{cases} \tag{3}$$

where $\boldsymbol{u}_f$ and p_f are the fluid velocity and pressure, respectively, $\boldsymbol{\sigma}_f = 2\mu_f\boldsymbol{\varepsilon}(\boldsymbol{u}_f) - p_f\boldsymbol{I}$ is the fluid stress tensor and $\boldsymbol{h}_f$ is (a regular enough) body force per unit mass exerted on the fluid. In (3), $\boldsymbol{g}_f^D, \boldsymbol{g}_f^N$ and $\boldsymbol{u}_{f0}$ are regular enough boundary and initial conditions, respectively. The first equation in (3) represents the conservation of total momentum of the flow, while the second the mass conservation. In this paper, we consider a different formulation of the Stokes problem, which is more convenient to accurately represent the momentum conservation and formulate the coupling conditions that will be discussed later. To this aim, we define

$$\boldsymbol{\Sigma}_f(t) := \int_0^t \boldsymbol{\sigma}_f(s)\,ds, \tag{4}$$

and integrate in time over $(0, t)$ the first equation in (3) to get

$$\boldsymbol{u}_f(t) - \rho_f^{-1}\nabla\cdot\boldsymbol{\Sigma}_f(t) = \int_0^t \boldsymbol{h}_f(s)\,ds + \boldsymbol{u}_{f0}. \tag{5}$$

Using now definition (4) we can infer that

$$\frac{1}{2\mu_f}\mathrm{dev}(\dot{\boldsymbol{\Sigma}}_f) = \boldsymbol{\varepsilon}(\boldsymbol{u}_f), \tag{6}$$

which directly encodes the incompressibility constraint (second equation) in (3). Next, by introducing the rotation $\boldsymbol{r}_f = \nabla \boldsymbol{u}_f - \boldsymbol{\varepsilon}(\boldsymbol{u}_f)$ and combining (5) and (6) we get

$$\begin{cases} (2\mu_f)^{-1}\mathrm{dev}(\dot{\boldsymbol{\Sigma}}_f) - \nabla(\rho_f^{-1}\nabla\cdot\boldsymbol{\Sigma}_f) + \boldsymbol{r}_f = \boldsymbol{F}_f, & in\ \Omega_f\times(0,T],\\ \mathrm{skew}(\dot{\boldsymbol{\Sigma}}_f) = \boldsymbol{0}, & in\ \Omega_f\times(0,T],\\ \rho_f^{-1}\nabla\cdot\boldsymbol{\Sigma}_f = \boldsymbol{G}_f, & on\ \Gamma_f^D\times(0,T],\\ \boldsymbol{\Sigma}_f\boldsymbol{n}_f = \int_0^t \boldsymbol{g}_f^N(s)\,ds, & on\ \Gamma_f^N\times(0,T],\\ \boldsymbol{\Sigma}_f = \boldsymbol{0}, & in\ \Omega_f\times\{0\}, \end{cases} \tag{7}$$

$$\text{with } \boldsymbol{F}_f = \nabla\left(\int_0^t \boldsymbol{h}_f(s)\,ds + \boldsymbol{u}_{f0}\right) \text{ and } \boldsymbol{G}_f = \boldsymbol{g}_f^D - \left(\int_0^t \boldsymbol{h}_f(s)\,ds - \boldsymbol{u}_{f0}\right)_{|\partial\Omega_f}.$$

The idea of introducing an additional variable to weakly enforce the symmetry of the stress field has been previously considered in the context of transient problems, e.g., in [47] and [48].

The poroelastic-fluid coupling is achieved by imposing interface conditions that must account for the conservation of mass and overall momentum. Therefore, these conditions will encompass the continuity of both the normal fluid flux and the stress. Two additional constitutive relations are involved: one describes the relationship between the filtration velocity and the pressure increment, the other addresses the impact of the tangential stress component on the velocity increment. The former is the Robin boundary condition, while the latter is the Beavers-Joseph-Saffman (BJS) slip condition. Hence, on $\Gamma_I\times(0,T]$ we impose:

$$\begin{cases} (\alpha\dot{\boldsymbol{u}}_p + \dot{\boldsymbol{w}}_p)\cdot\boldsymbol{n}_p = \boldsymbol{u}_f\cdot\boldsymbol{n}_p, (\text{flux conservation}),\\ \dot{\boldsymbol{\Sigma}}_f\boldsymbol{n}_p\cdot\boldsymbol{n}_p = \gamma\dot{\boldsymbol{w}}_p\cdot\boldsymbol{n}_p - \dot{p}_p, (\text{Robin condition}),\\ \alpha\dot{\boldsymbol{\Sigma}}_f\boldsymbol{n}_p\cdot\boldsymbol{n}_p = \boldsymbol{\sigma}_p\boldsymbol{n}_p\cdot\boldsymbol{n}_p, (\text{normal stress conservation}),\\ \dot{\boldsymbol{\Sigma}}_f\boldsymbol{n}_p\wedge\boldsymbol{n}_p = \boldsymbol{\sigma}_p\boldsymbol{n}_p\wedge\boldsymbol{n}_p = \delta(\boldsymbol{u}_f - \dot{\boldsymbol{u}}_p)\wedge\boldsymbol{n}_p, (\text{BJS condition}). \end{cases} \tag{8}$$

Here $\alpha > 0$ is a coefficient related to the fraction of the contact surface Γ_I where the diffusion paths of the porous medium are exposed to the fluid in the open channel, $\gamma \geq 0$ is the fluid entry resistance and $\delta > 0$ depends on the slip rate coefficient and the conductivity tensor. Furthermore, for a vector field $\boldsymbol{v}$ defined on Γ_I, the notation $\boldsymbol{v}\wedge\boldsymbol{n}_p$ denotes the tangential component of $\boldsymbol{v}$. In the case $d = 2$, we have $\boldsymbol{v}\wedge\boldsymbol{n}_p = \boldsymbol{v}\cdot\boldsymbol{t}_p$, where $\boldsymbol{t}_p$ is the tangential unit vector to the interface Γ_I, directed in such a way that the angle measured from $\boldsymbol{t}_p$ to $\boldsymbol{n}_p$ is positive.

Finally, the poroelastic-fluid interaction problem is obtained by combining (1) and (7) with conditions (8).

2.3 Weak formulation

For the sake of presentation, in the following, we will consider $\boldsymbol{g}_p^N = \boldsymbol{0}$, $q_p^N = 0$ on Γ_p^N in (1) and $\boldsymbol{g}_f^D = \boldsymbol{g}_f^N = \boldsymbol{0}$ on Γ_f^N in (7). The general case can be treated analogously. We introduce the Sobolev space

$$\boldsymbol{V} := \boldsymbol{H}^1_{0,\Gamma_p^D}(\Omega_p)\times\boldsymbol{H}_{0,\Gamma_p^D}(\mathrm{div},\Omega_p)\times\mathbb{H}_{0,\Gamma_f^N}(\mathrm{div},\Omega_f)\times[L^2(\Omega_f)]^{d^*},$$

with $d^* = 1$ for $d = 2$ and $d^* = 3$ for $d = 3$ corresponding to the dimension of skew-symmetric matrices in $\mathbb{R}^{d\times d}$. Then, the weak formulation of Biot–Stokes system reads as follows: $\forall t\in(0,T]$, find $(\boldsymbol{u}_p,\boldsymbol{w}_p,\boldsymbol{\Sigma}_f,\boldsymbol{r}_f)(t)\in\boldsymbol{V}$ such that $\forall(\boldsymbol{v},\boldsymbol{z},\boldsymbol{\tau},\boldsymbol{\lambda})\in\boldsymbol{V}$ it holds

$$\begin{aligned} &\mathcal{M}^p((\ddot{\boldsymbol{u}}_p,\ddot{\boldsymbol{w}}_p),(\boldsymbol{v},\boldsymbol{z})) + \mathcal{M}^f(\dot{\boldsymbol{\Sigma}}_f,\boldsymbol{\tau}) + \mathcal{D}^p(\dot{\boldsymbol{w}}_p,\boldsymbol{z}) + \mathcal{D}^f(\dot{\boldsymbol{\Sigma}}_f,\boldsymbol{\tau})\\ &\quad + \mathcal{A}^p((\boldsymbol{u}_p,\boldsymbol{w}_p),(\boldsymbol{v},\boldsymbol{z})) + \mathcal{A}^f(\boldsymbol{\Sigma}_f,\boldsymbol{\tau}) + \mathcal{B}^f(\boldsymbol{r}_f,\boldsymbol{\tau}) - \mathcal{B}^f(\boldsymbol{\lambda},\dot{\boldsymbol{\Sigma}}_f)\\ &\quad + \mathcal{C}^{pf}((\dot{\boldsymbol{u}}_p,\dot{\boldsymbol{w}}_p),\boldsymbol{\tau}) - \mathcal{C}^{fp}(\dot{\boldsymbol{\Sigma}}_f,(\boldsymbol{v},\boldsymbol{z})) = \mathcal{F}(\boldsymbol{v},\boldsymbol{z},\boldsymbol{\tau}) \end{aligned} \tag{9}$$

with initial conditions given as in (1) and (7) and where for any $\boldsymbol{u},\boldsymbol{v}\in\boldsymbol{H}^1_{0,\Gamma_p^D}(\Omega_p)$, $\boldsymbol{w},\boldsymbol{z}\in\boldsymbol{H}_{0,\Gamma_p^D}(\mathrm{div},\Omega_p)$, $\boldsymbol{\Sigma},\boldsymbol{\tau}\in\mathbb{H}_{0,\Gamma_f^N}(\mathrm{div},\Omega_f)$, and $\boldsymbol{r},\boldsymbol{\lambda}\in[L^2(\Omega_f)]^{d^*}$ we have

$$\begin{aligned} \mathcal{M}^p((\boldsymbol{u},\boldsymbol{w}),(\boldsymbol{v},\boldsymbol{z})) &:= (\rho\boldsymbol{u},\boldsymbol{v})_{\Omega_p} + (\rho_f\boldsymbol{w},\boldsymbol{v})_{\Omega_p} + (\rho_f\boldsymbol{u},\boldsymbol{z})_{\Omega_p} + (\rho_w\boldsymbol{w},\boldsymbol{z})_{\Omega_p},\\ \mathcal{M}^f(\boldsymbol{\Sigma},\boldsymbol{\tau}) &:= ((2\mu_f)^{-1}\mathrm{dev}(\boldsymbol{\Sigma}),\mathrm{dev}(\boldsymbol{\tau}))_{\Omega_f},\\ \mathcal{D}^p(\boldsymbol{w},\boldsymbol{z}) &:= (\eta k^{-1}\boldsymbol{w},\boldsymbol{z})_{\Omega_p} + \langle\gamma\boldsymbol{w}\cdot\boldsymbol{n}_p,\boldsymbol{z}\cdot\boldsymbol{n}_p\rangle_{\Gamma_I},\\ \mathcal{D}^f(\boldsymbol{\Sigma},\boldsymbol{\tau}) &:= (\delta^{-1}\boldsymbol{\Sigma}\boldsymbol{n}_p\wedge\boldsymbol{n}_p,\boldsymbol{\tau}\boldsymbol{n}_p\wedge\boldsymbol{n}_p)_{\Gamma_I},\\ \mathcal{A}^p((\boldsymbol{u},\boldsymbol{w}),(\boldsymbol{v},\boldsymbol{z})) &:= (\boldsymbol{\sigma}_e(\boldsymbol{u}),\boldsymbol{\varepsilon}(\boldsymbol{v}))_{\Omega_p} + (m(\beta\nabla\cdot\boldsymbol{u} + \nabla\cdot\boldsymbol{w}),\beta\nabla\cdot\boldsymbol{v} + \nabla\cdot\boldsymbol{z})_{\Omega_p},\\ \mathcal{A}^f(\boldsymbol{\Sigma},\boldsymbol{\tau}) &:= (\rho_f^{-1}\nabla\cdot\boldsymbol{\Sigma},\nabla\cdot\boldsymbol{\tau})_{\Omega_f},\\ \mathcal{B}^f(\boldsymbol{r},\boldsymbol{\tau}) &:= (\boldsymbol{r},\mathrm{skew}(\boldsymbol{\tau}))_{\Omega_f},\\ C^{pf}((\boldsymbol{u},\boldsymbol{w}),\boldsymbol{\tau}) &:= \langle(\alpha\boldsymbol{u}+\boldsymbol{w})\cdot\boldsymbol{n}_p,\boldsymbol{\tau}\boldsymbol{n}_p\cdot\boldsymbol{n}_p\rangle_{\Gamma_I} + \langle\boldsymbol{u}\wedge\boldsymbol{n}_p,\boldsymbol{\tau}\boldsymbol{n}_p\wedge\boldsymbol{n}_p\rangle_{\Gamma_I},\\ C^{fp}(\boldsymbol{\Sigma},(\boldsymbol{v},\boldsymbol{z})) &:= \langle\boldsymbol{\Sigma}\boldsymbol{n}_p\cdot\boldsymbol{n}_p,(\alpha\boldsymbol{v}+\boldsymbol{z})\cdot\boldsymbol{n}_p\rangle_{\Gamma_I} + \langle\boldsymbol{\Sigma}\boldsymbol{n}_p\wedge\boldsymbol{n}_p,\boldsymbol{v}\wedge\boldsymbol{n}_p\rangle_{\Gamma_I},\\ \mathcal{F}(\boldsymbol{v},\boldsymbol{z},\boldsymbol{\tau}) &:= (\boldsymbol{f}_p,\boldsymbol{v})_{\Omega_p} + (\boldsymbol{g}_p,\boldsymbol{z})_{\Omega_p} + (\boldsymbol{F}_f,\boldsymbol{\tau})_{\Omega_f} - \langle\boldsymbol{G}_f,\boldsymbol{\tau}\boldsymbol{n}_f\rangle_{\Gamma_I\cup\Gamma_f^D}, \end{aligned} \tag{10}$$

where $\langle\cdot,\cdot\rangle_{\Gamma_I}$ denotes the $H^{\frac{1}{2}}(\Gamma_I)$ - $H^{-\frac{1}{2}}(\Gamma_I)$ duality product. We also remark that, according to the assumption $\boldsymbol{g}_f^D = \boldsymbol{0}$ and integration by parts, we can rewrite the third and fourth terms appearing in the definition of the linear functional $\mathcal{F}$ to obtain the alternative expression

$$\mathcal{F}(\boldsymbol{v},\boldsymbol{z},\boldsymbol{\tau}) = (\boldsymbol{f}_p,\boldsymbol{v})_{\Omega_p} + (\boldsymbol{g}_p,\boldsymbol{z})_{\Omega_p} - \left(\int_0^t \boldsymbol{h}_f(s)\,ds + \boldsymbol{u}_{f0},\nabla\cdot\boldsymbol{\tau}\right)_{\Omega_f}.$$

This shows, in particular, that standard regularity requirements on the forcing term $\boldsymbol{h}_f$ and initial velocity $\boldsymbol{u}_{f0}$ are sufficient for the definition of problem (9). We refer to [12] and [26] for the well-posedness of an unsteady Stokes–Biot coupled problem and of low-frequency poroelasticity coupled to acoustic wave propagation in the framework of Hille-Yosida theory. The well-posedness of the initial boundary value problem in (9) can be obtained by adapting the arguments therein. However, for the sake of brevity, we omit the details and focus here on the design of the spatial discretization.

2.4 Stability analysis

This section presents the stability analysis for the continuous problem (9). The arguments in the proof of the main theorem will also be used in the discrete setting in Sect. 3. For any $(\boldsymbol{u}, \boldsymbol{w}, \boldsymbol{\Sigma}) \in C^1([0,T]; \boldsymbol{H}^1_{0,\Gamma_p^D}(\Omega_p) \times \boldsymbol{H}_{0,\Gamma_p^D}(\mathrm{div}, \Omega_p) \times \mathbb{H}_{0,\Gamma_f^N}(\mathrm{div}, \Omega_f))$ we introduce the energy norms

$$
\begin{aligned}
\|(\boldsymbol{u},\boldsymbol{w},\boldsymbol{\Sigma})(t)\|^2_{\mathcal{E}} &:= \|(\boldsymbol{u},\boldsymbol{w})(t)\|^2_{\mathcal{E}_p} + \|\boldsymbol{\Sigma}(t)\|^2_{\mathcal{E}_f},\\
\|(\boldsymbol{u},\boldsymbol{w})(t)\|^2_{\mathcal{E}_p} &:= \|\dot{\boldsymbol{u}}(t)\|^2_{\Omega_p} + \|\dot{\boldsymbol{w}}(t)\|^2_{\Omega_p} + \|(\eta/k)^{\frac{1}{2}}\boldsymbol{w}(t)\|^2_{\Omega_p} + \|\gamma^{\frac{1}{2}}\boldsymbol{w}\cdot\boldsymbol{n}_p(t)\|^2_{\Gamma_I} + \|\mathbb{C}^{\frac{1}{2}}\boldsymbol{\varepsilon}(\boldsymbol{u})(t)\|^2_{\Omega_p}\\
&\quad + \|m^{\frac{1}{2}}\nabla\cdot(\beta\boldsymbol{u}+\boldsymbol{w})(t)\|^2_{\Omega_p},\\
\|\boldsymbol{\Sigma}(t)\|^2_{\mathcal{E}_f} &:= \|(2\mu_f)^{-\frac{1}{2}}\mathrm{dev}(\boldsymbol{\Sigma})(t)\|^2_{\Omega_f} + \|\rho_f^{-\frac{1}{2}}\nabla\cdot\boldsymbol{\Sigma}(t)\|^2_{\Omega_f} + \|\delta^{-\frac{1}{2}}\boldsymbol{\Sigma}\boldsymbol{n}_p\wedge\boldsymbol{n}_p(t)\|^2_{\Gamma_I}.
\end{aligned}
$$

Lemma 1 The bilinear forms $\mathcal{M}^p$, $\mathcal{A}^p$, and $\mathcal{D}^p$ defined in (10) are such that for any $\boldsymbol{u}, \boldsymbol{v} \in \boldsymbol{H}^1_{0,\Gamma_p^D}(\Omega_p)$ and any $\boldsymbol{w}, \boldsymbol{z} \in \boldsymbol{H}_{0,\Gamma_p^D}(\mathrm{div}, \Omega_p)$ it holds

$$
\mathcal{M}^p((\boldsymbol{u},\boldsymbol{w}),(\boldsymbol{v},\boldsymbol{z})) \lesssim (\|\boldsymbol{u}\|_{\Omega_p} + \|\boldsymbol{w}\|_{\Omega_p})(\|\boldsymbol{v}\|_{\Omega_p} + \|\boldsymbol{z}\|_{\Omega_p}), \tag{11}
$$

$$
\mathcal{M}^p((\boldsymbol{u},\boldsymbol{w}),(\boldsymbol{u},\boldsymbol{w})) \gtrsim \|\boldsymbol{u}\|^2_{\Omega_p} + \|\boldsymbol{w}\|^2_{\Omega_p}, \tag{12}
$$

$$
\mathcal{A}^p((\boldsymbol{u},\boldsymbol{w}),(\boldsymbol{v},\boldsymbol{z})) + \mathcal{D}^p(\boldsymbol{w},\boldsymbol{z}) \lesssim \|\boldsymbol{u}\|_{1,\Omega_p}\|\boldsymbol{v}\|_{1,\Omega_p} + \|\boldsymbol{w}\|_{\mathrm{div},\Omega_p}\|\boldsymbol{z}\|_{\mathrm{div},\Omega_p}, \tag{13}
$$

$$
\mathcal{A}^p((\boldsymbol{u},\boldsymbol{w}),(\boldsymbol{u},\boldsymbol{w})) + \mathcal{D}^p(\boldsymbol{w},\boldsymbol{w}) \gtrsim \|\boldsymbol{u}\|^2_{1,\Omega_p} + \|\boldsymbol{w}\|^2_{\mathrm{div},\Omega_p}. \tag{14}
$$

Proof See [26, Lemma 2.3]. □

Lemma 2 The bilinear forms $\mathcal{M}^f$ and $\mathcal{A}^f$ defined in (10) are such that for any $\boldsymbol{\Sigma}, \boldsymbol{\tau} \in \mathbb{H}_{0,\Gamma_f^N}(\mathrm{div}, \Omega_f)$

$$
\mathcal{M}^f(\boldsymbol{\Sigma},\boldsymbol{\tau}) + \mathcal{A}^f(\boldsymbol{\Sigma},\boldsymbol{\tau}) \lesssim \|\boldsymbol{\Sigma}\|_{\mathrm{div},\Omega_f}\|\boldsymbol{\tau}\|_{\mathrm{div},\Omega_f}, \tag{15}
$$

$$
\mathcal{M}^f(\boldsymbol{\Sigma},\boldsymbol{\Sigma}) + \mathcal{A}^f(\boldsymbol{\Sigma},\boldsymbol{\Sigma}) \gtrsim \|\boldsymbol{\Sigma}\|^2_{\mathrm{div},\Omega_f},. \tag{16}
$$

Proof The continuity in (15) directly follows from the definition of the deviatoric operator, whereas for (16) we refer the reader to [27, Lemma 2.2]. □

Theorem 1 For any time $t \in (0,T]$ let $(\boldsymbol{u}_p, \boldsymbol{w}_p, \boldsymbol{\Sigma}_f, \boldsymbol{r}_f)(t) \in \boldsymbol{V}$ be the solution to problem (9). Then, it holds

$$
\sup_{t\in(0,T]} \|(\boldsymbol{u}_p,\boldsymbol{w}_p,\boldsymbol{\Sigma}_f)(t)\|_{\mathcal{E}} \lesssim \mathcal{G}_0 + \int_0^T \mathcal{N}(\boldsymbol{f}_p,\boldsymbol{g}_p,\boldsymbol{F}_f,\boldsymbol{G}_f)(s)\,ds,
$$

where

$$
\mathcal{G}_0^2 := \|(\boldsymbol{u}_p,\boldsymbol{w}_p,\boldsymbol{\Sigma}_f)(0)\|^2_{\mathcal{E}} + \sup_{t\in[0,T]}\left(\|\boldsymbol{F}_f(t)\|^2_{\Omega_f} + \|\boldsymbol{G}_f(t)\|^2_{\Gamma_I\cup\Gamma_f^D}\right), \tag{17}
$$

$$
\mathcal{N}(\boldsymbol{f}_p,\boldsymbol{g}_p,\boldsymbol{F}_f,\boldsymbol{G}_f)(t) := \|\boldsymbol{f}_p(t)\|_{\Omega_p} + \|\boldsymbol{g}_p(t)\|_{\Omega_p} + \|\dot{\boldsymbol{H}}_f(t)\|_{\Omega_f} + \|\dot{\boldsymbol{G}}_f(t)\|_{\Gamma_I\cup\Gamma_f^D}. \tag{18}
$$

Proof We consider $(\boldsymbol{v},\boldsymbol{z},\boldsymbol{\tau},\boldsymbol{\lambda}) = (\dot{\boldsymbol{u}}_p, \dot{\boldsymbol{w}}_p, \dot{\boldsymbol{\Sigma}}_f, \boldsymbol{r}_f)$ in (9) to get

$$
\begin{aligned}
&\mathcal{M}^p((\ddot{\boldsymbol{u}}_p,\ddot{\boldsymbol{w}}_p),(\dot{\boldsymbol{u}}_p,\dot{\boldsymbol{w}}_p)) + \mathcal{M}^f(\dot{\boldsymbol{\Sigma}}_f,\dot{\boldsymbol{\Sigma}}_f) + \mathcal{D}^p(\dot{\boldsymbol{w}}_p,\dot{\boldsymbol{w}}_p) + \mathcal{D}^f(\dot{\boldsymbol{\Sigma}}_f,\dot{\boldsymbol{\Sigma}}_f)\\
&\quad + \mathcal{A}^p((\boldsymbol{u}_p,\boldsymbol{w}_p),(\dot{\boldsymbol{u}}_p,\dot{\boldsymbol{w}}_p)) + \mathcal{A}^f(\boldsymbol{\Sigma}_f,\dot{\boldsymbol{\Sigma}}_f) = \mathcal{F}(\dot{\boldsymbol{u}}_p,\dot{\boldsymbol{w}}_p,\dot{\boldsymbol{\Sigma}}_f).
\end{aligned}
$$

Integrating in time between 0 and t the above equation leads to

$$
\begin{aligned}
&\frac{1}{2}\mathcal{M}^p((\dot{\boldsymbol{u}}_p,\dot{\boldsymbol{w}}_p),(\dot{\boldsymbol{u}}_p,\dot{\boldsymbol{w}}_p))(t) + \int_0^t \mathcal{D}^p(\dot{\boldsymbol{w}}_p,\dot{\boldsymbol{w}}_p)(s)\,ds + \frac{1}{2}\mathcal{A}^p((\boldsymbol{u}_p,\boldsymbol{w}_p),(\boldsymbol{u}_p,\boldsymbol{w}_p))(t)\\
&+ \int_0^t \mathcal{M}^f(\dot{\boldsymbol{\Sigma}}_f,\dot{\boldsymbol{\Sigma}}_f)(s)\,ds + \frac{1}{2}\mathcal{A}^f(\boldsymbol{\Sigma}_f,\boldsymbol{\Sigma}_f)(t) + \int_0^t \mathcal{D}^f(\dot{\boldsymbol{\Sigma}}_f,\dot{\boldsymbol{\Sigma}}_f)(s)\,ds\\
&= \int_0^t \mathcal{F}(\dot{\boldsymbol{u}}_p,\dot{\boldsymbol{w}}_p,\dot{\boldsymbol{\Sigma}}_f)(s)\,ds + \frac{1}{2}\mathcal{M}^p((\boldsymbol{v}_{p0},\boldsymbol{z}_{p0}),(\boldsymbol{v}_{p0},\boldsymbol{z}_{p0}))\\
&\quad + \frac{1}{2}\mathcal{A}^p((\boldsymbol{u}_{p0},\boldsymbol{w}_{p0}),(\boldsymbol{u}_{p0},\boldsymbol{w}_{p0})) + \frac{1}{2}\mathcal{A}^f(\boldsymbol{\Sigma}_{f0},\boldsymbol{\Sigma}_{f0}).
\end{aligned}
$$

Next, using that $\mathcal{B}(\boldsymbol{\psi},\boldsymbol{\psi})(t) \lesssim \mathcal{B}(\boldsymbol{\psi},\boldsymbol{\psi})(0) + \int_0^t \mathcal{B}(\dot{\boldsymbol{\psi}},\dot{\boldsymbol{\psi}})(s)\,ds$ for $\mathcal{B}(\cdot,\cdot) = \{\mathcal{D}^p(\cdot,\cdot), \mathcal{D}^f(\cdot,\cdot), \mathcal{M}^f(\cdot,\cdot)\}$ with $\boldsymbol{\psi} = \{\boldsymbol{w}, \boldsymbol{\Sigma}, \dot{\boldsymbol{\Sigma}}\}$, respectively, together with (11)-(12), (13)-(14) and (15)-(16), we obtain

$$
\|(\boldsymbol{u},\boldsymbol{w})(t)\|^2_{\mathcal{E}_p} + \|\boldsymbol{\Sigma}(t)\|^2_{\mathcal{E}_f} \lesssim \int_0^t \mathcal{F}(\dot{\boldsymbol{u}}_p,\dot{\boldsymbol{w}}_p,\dot{\boldsymbol{\Sigma}}_f)(s)\,ds + \|(\boldsymbol{u}_{p0},\boldsymbol{w}_{p0})\|^2_{\mathcal{E}_p} + \|\boldsymbol{\Sigma}_{f0}\|^2_{\mathcal{E}_f}. \tag{19}
$$

Then, we apply the Cauchy-Schwarz inequality for the forcing terms in the porous domain, while we integrate by parts the other terms to get

$$
\begin{aligned}
\int_0^t \mathcal{F}(\dot{\boldsymbol{u}}_p,\dot{\boldsymbol{w}}_p,\dot{\boldsymbol{\Sigma}}_f)(s)\,ds &\lesssim \int_0^t (\|\boldsymbol{f}_p(s)\|_{\Omega_p} + \|\boldsymbol{g}_p(s)\|_{\Omega_p})\|(\boldsymbol{u}_p,\boldsymbol{w}_p)(s)\|_{\mathcal{E}_p}\,ds\\
&+ (\boldsymbol{F}_f,\boldsymbol{\Sigma}_f)_{\Omega_f}(t) - (\boldsymbol{F}_f,\boldsymbol{\Sigma}_f)_{\Omega_f}(0) - \int_0^t (\dot{\boldsymbol{F}}_f,\boldsymbol{\Sigma}_f)_{\Omega_f}(s)\,ds\\
&- \langle \boldsymbol{G}_f,\boldsymbol{\Sigma}_f\boldsymbol{n}_p\rangle_{\Gamma_I\cup\Gamma_f^D}(t) + \langle \boldsymbol{G}_f,\boldsymbol{\Sigma}_f\boldsymbol{n}_p\rangle_{\Gamma_I\cup\Gamma_f^D}(0) + \int_0^t \langle \dot{\boldsymbol{G}}_f,\boldsymbol{\Sigma}_f\boldsymbol{n}_p\rangle_{\Gamma_I\cup\Gamma_f^D}(s)\,ds.
\end{aligned}
$$

Applying again the Cauchy-Schwarz and Young inequalities, using the trace inequality in $\mathbb{H}(\mathrm{div},\Omega_f)$ together with [27, Lemma 2.2], and recalling that $\boldsymbol{\Sigma}_f|_{t=0} = \boldsymbol{0}$, we obtain

$$
\begin{aligned}
\int_0^t \mathcal{F}(\dot{\boldsymbol{u}}_p,\dot{\boldsymbol{w}}_p,\dot{\boldsymbol{\Sigma}}_f)(s)\,ds &\lesssim \int_0^t (\|\boldsymbol{f}_p(s)\|_{\Omega_p} + \|\boldsymbol{g}_p(s)\|_{\Omega_p})\|(\boldsymbol{u}_p,\boldsymbol{w}_p)(s)\|_{\mathcal{E}_p}\,ds\\
&+ \frac{1}{2\epsilon}\|\boldsymbol{F}_f(t)\|^2_{\Omega_f} + \frac{1}{2\epsilon}\|\boldsymbol{G}_f(t)\|^2_{\Gamma_I\cup\Gamma_f^D} + \epsilon\|\boldsymbol{\Sigma}_f(t)\|^2_{\mathcal{E}_f}\\
&+ \int_0^t \left(\|\dot{\boldsymbol{F}}_f(s)\|_{\Omega_f}\|\boldsymbol{\Sigma}_f(s)\|_{\mathcal{E}_f} + \|\dot{\boldsymbol{G}}_f(s)\|_{\Gamma_I\cup\Gamma_f^D}\|\boldsymbol{\Sigma}_f(s)\|_{\mathcal{E}_f}\right)ds.
\end{aligned}
$$

Plugging the above estimate into (19) and choosing ϵ small enough, we get

$$
\|(\boldsymbol{u},\boldsymbol{w})(t)\|^2_{\mathcal{E}_p} + \|\boldsymbol{\Sigma}(t)\|^2_{\mathcal{E}_f} \lesssim \mathcal{G}_0^2 + \int_0^t \mathcal{N}(\boldsymbol{f}_p,\boldsymbol{g}_p,\boldsymbol{F}_f,\boldsymbol{G}_f)\left(\|(\boldsymbol{u},\boldsymbol{w})(s)\|_{\mathcal{E}_p} + \|\boldsymbol{\Sigma}(s)\|_{\mathcal{E}_f}\right)ds
$$

with $\mathcal{G}_0$ and $\mathcal{N}$ defined as in (17) and (18), respectively. Finally, we prove the assertion by taking the supremum over

$t \in (0, T]$ and applying Gronwall's Lemma [49, Lemma 2.2]. □

3 Discontinuous Galerkin space discretization

In this section, we present the PolydG discretization of the coupled problem consisting of systems (1), (7) and (8).

3.1 Preliminaries

We introduce a polytopic mesh $\mathcal{T}_h$ made of general polygons or polyhedra in two or three dimensions, respectively, and define $\mathcal{T}_h$ as $\mathcal{T}_h = \mathcal{T}_h^p \cup \mathcal{T}_h^f$, where $\mathcal{T}_h^\diamond = \{K \in \mathcal{T}_h : \overline{K} \subseteq \overline{\Omega}_\diamond\}$, with $\diamond = \{p, f\}$. We assume that the meshes $\mathcal{T}_h^p$ and $\mathcal{T}_h^f$ are aligned with Ω_p and Ω_f, respectively. We set the polynomial degrees $p_{p,K} \geq 1$ and $p_{f,K} \geq 1$ in each mesh element of $\mathcal{T}_h^p$ and $\mathcal{T}_h^f$. Following [29, Section 6.2] we introduce the discrete polynomial spaces:

$$\boldsymbol{V}_h^p := [\mathcal{P}_{p_p}(\mathcal{T}_h^p)]^d,\ \boldsymbol{S}_h^f := [\mathcal{P}_{p_f}(\mathcal{T}_h^f)]^{d\times d} \text{ and } \boldsymbol{\Lambda}_h^f := [\mathcal{P}_{p_f-1}(\mathcal{T}_h^f)]^{d^*}.$$

Moreover, $\mathcal{P}_r(\mathcal{T}_h^\diamond)$ is the space of piecewise polynomials in $\Omega_\diamond$ of total degree less than or equal to r in any $K \in \mathcal{T}_h^\diamond$ with $\diamond = \{p, f\}$.

In the following, we assume that the model parameters in (1) and (7) are element-wise constant for all $K \in \mathcal{T}_h^p \cup \mathcal{T}_h^f$. To deal with polygonal and polyhedral elements, we define *element-interface* the intersection of the $(d-1)$-dimensional faces of any two neighboring elements of $\mathcal{T}_h$. If $d = 2$, an interface/face is a line segment and the set of all interfaces/faces is denoted by $\mathcal{F}_h$. If $d = 3$, an interface is a polygon we assume could be further decomposed into planar triangles collected in the set $\mathcal{F}_h$. We decompose $\mathcal{F}_h$ as $\mathcal{F}_h = \mathcal{F}_h^I \cup \mathcal{F}_h^p \cup \mathcal{F}_h^f$, where $\mathcal{F}_h^I = \{F \in \mathcal{F}_h : F \subset \partial K^p \cap \partial K^f, K^p \in \mathcal{T}_h^p, K^f \in \mathcal{T}_h^f\}$, and $\mathcal{F}_h^p$, and $\mathcal{F}_h^f$ denote all the faces of $\mathcal{T}_h^p$, and $\mathcal{T}_h^f$ respectively, not laying on Γ_I. Finally, the faces of $\mathcal{T}_h^p$ and $\mathcal{T}_h^f$ can be further written as the union of *internal* (i) and *boundary* (b) faces, respectively, namely, $\mathcal{F}_h^p = \mathcal{F}_h^{p,i} \cup \mathcal{F}_h^{p,b}$ and $\mathcal{F}_h^f = \mathcal{F}_h^{f,i} \cup \mathcal{F}_h^{f,b}$, where $\mathcal{F}_h^{\diamond,b} = \mathcal{F}_h^{\diamond,N} \cup \mathcal{F}_h^{\diamond,D}$, with $\diamond = \{p, f\}$, include both the edges where Neumann and Dirichlet conditions are imposed. Following [29], we next introduce the main assumption on $\mathcal{T}_h$.

Definition 1 A mesh $\mathcal{T}_h$ is said to be *polytopic-regular* if there exist a constant $C_{\text{reg}} > 0$ such that, for any $K \in \mathcal{T}_h$, there exists a set of non-overlapping d-dimensional simplices contained in K, denoted by $\{S_K^F\}_{F\subset\partial K}$, fulfilling the inequality $h_K \leq C_{\text{reg}} d |S_K^F| \, |F|^{-1}$ for any face $F \subset \partial K$, with the constant C_{reg} being independent of the number of faces per element and the face measures.

Assumption 1 The mesh $\mathcal{T}_h$ satisfies the following assumptions:

(a) The sequence of meshes $\{\mathcal{T}_h\}_h$ is assumed to be *uniformly* polytopic regular in the sense of Definition 1, namely the constant C_{reg} appearing in Definition 1 does not depend on h.
(b) For any pair of neighboring elements $K^\pm \in \mathcal{T}_h^\diamond$, it holds $h_{K^+} \lesssim h_{K^-} \lesssim h_{K^+}$, $p_{\diamond,K^+} \lesssim p_{\diamond,K^-} \lesssim p_{\diamond,K^+}$, with $\diamond = \{e, p\}$.

This will allow us to avoid technicalities in the following proofs. We remark that these assumptions do not restrict the number of faces per element or their measure relative to the diameter of the element they belong to as pointed out in [29]. Under Assumption 1, we have that $|F| \lesssim |K|^{1/2}$ for any element $K \in \mathcal{T}_h$ and face $F \subset \partial K$, thus the following *trace-inverse inequality* holds [50]:

$$||v||_{L^2(\partial K)} \lesssim p h_K^{-1/2} ||v||_{L^2(K)} \quad \forall\, K \in \mathcal{T}_h\ \forall v \in \mathcal{P}_p(K). \tag{20}$$

Next, we make the following assumption for later use.

Assumption 2 Any mesh $\mathcal{T}_h$ admits a covering $\mathcal{T}_\S$ in the sense of Definition 1 such that i) $\max_{K\in\mathcal{T}_h} \text{card}\{K' \in \mathcal{T}_h : K' \cap \mathcal{K} \neq \emptyset,\ \mathcal{K} \in \mathcal{T}_\S \text{ s.t. } K \subset \mathcal{K}\} \lesssim 1$ and ii) $h_\mathcal{K} \lesssim h_K$ for each pair $K \in \mathcal{T}_h$, $\mathcal{K} \in \mathcal{T}_\S$ with $K \subset \mathcal{K}$.

Finally, as in [51], for sufficiently piecewise smooth scalar-, vector-, and tensor-valued versions ψ, $\boldsymbol{v}$ and $\boldsymbol{\tau}$, respectively, we define the averages and jumps on each *element-interface* $F \in \mathcal{F}_h^{p,i} \cup \mathcal{F}_h^{f,i} \cup \mathcal{F}_h^I$ shared by the elements $K^\pm \in \mathcal{T}_h$ as follows:

$$\{\psi\} := \frac{\psi^+ + \psi^-}{2}, \qquad [[\psi]] := \psi^+ \boldsymbol{n}^+ + \psi^- \boldsymbol{n}^-,$$
$$\{\boldsymbol{v}\} := \frac{\boldsymbol{v}^+ + \boldsymbol{v}^-}{2}, \qquad [[\boldsymbol{v}]] := \boldsymbol{v}^+ \otimes \boldsymbol{n}^+ + \boldsymbol{v}^- \otimes \boldsymbol{n}^-,$$
$$[[\boldsymbol{v}]]_{\boldsymbol{n}} := \boldsymbol{v}^+ \cdot \boldsymbol{n}^+ + \boldsymbol{v}^- \cdot \boldsymbol{n}^-,$$
$$\{\boldsymbol{\tau}\} := \frac{\boldsymbol{\tau}^+ + \boldsymbol{\tau}^-}{2}, \qquad [[\boldsymbol{\tau}]] := \boldsymbol{\tau}^+ \boldsymbol{n}^+ + \boldsymbol{\tau}^- \boldsymbol{n}^-,$$

where $\otimes$ is the tensor product in $\mathbb{R}^3$, $\cdot^\pm$ denotes the trace on F taken within $K^\pm$, and $\boldsymbol{n}^\pm$ is the outer normal vector to $\partial K^\pm$. Accordingly, on *boundary* faces $F \in \mathcal{F}_h^{p,b} \cup \mathcal{F}_h^{f,b}$, we set

$[[\psi]]:=\psi\boldsymbol{n}$, $\{\psi\}:=\psi$, $\{\boldsymbol{v}\}:=\boldsymbol{v}$, $[[\boldsymbol{v}]]:=\boldsymbol{v}\otimes\boldsymbol{n}$, $[[\boldsymbol{v}]]_{\boldsymbol{n}}:=\boldsymbol{v}\cdot\boldsymbol{n}$, $\{\boldsymbol{\tau}\}:=\boldsymbol{\tau}$,$[[\boldsymbol{\tau}]]:=\boldsymbol{\tau}\boldsymbol{n}$.

For later use, we also define ∇_h and $(\nabla_h\cdot)$ to be the broken gradient and divergence operators, respectively, set $\boldsymbol{\varepsilon}_h(\boldsymbol{v})=(\nabla_h\boldsymbol{v}+\nabla_h\boldsymbol{v}^T)/2$, and use the short-hand notation $(\cdot,\cdot)_{\Omega_\diamond}=\sum_{K\in\mathcal{T}_h^\diamond}(\cdot,\cdot)_K$ and $\langle\cdot,\cdot\rangle_{\mathcal{F}_h^\diamond}=\sum_{F\in\mathcal{F}_h^\diamond}\langle\cdot,\cdot\rangle_F$ for $\diamond=\{p,f\}$. In the following, we assume that $\mathbb{C}$, m and ρ_f are element-wise constant and we define $\overline{\mathbb{C}}_K=(|\mathbb{C}^{1/2}|_2^2)_{|K}$, $\overline{m}_K=(m)_{|K}$ for all $K\in\mathcal{T}_h^p$ and $\overline{\rho}_{f,K}=\rho_{f|K}$ for all $K\in\mathcal{T}_h^f$.

3.2 Semi-discrete polydG formulation

We define the discrete space $\boldsymbol{V}_h:=\boldsymbol{V}_h^p\times\boldsymbol{V}_h^p\times\boldsymbol{S}_h^f\times\boldsymbol{\Lambda}_h^f$ and introduce the semi-discrete problem: $\forall t\in(0,T]$, find $(\boldsymbol{u}_{ph},\boldsymbol{w}_{ph},\boldsymbol{\Sigma}_{fh},\boldsymbol{r}_{fh})(t)\in\boldsymbol{V}_h$ s. t. $\forall(\boldsymbol{v},\boldsymbol{z},\boldsymbol{\tau},\boldsymbol{\lambda})\in\boldsymbol{V}_h$ it holds

$$\begin{aligned}&\mathcal{M}^p((\ddot{\boldsymbol{u}}_{ph},\ddot{\boldsymbol{w}}_{ph}),(\boldsymbol{v},\boldsymbol{z}))+\mathcal{M}^f(\dot{\boldsymbol{\Sigma}}_{fh},\boldsymbol{\tau})+\mathcal{D}^p(\dot{\boldsymbol{w}}_{ph},\boldsymbol{z})+\mathcal{D}^f(\dot{\boldsymbol{\Sigma}}_{fh},\boldsymbol{\tau})\\&+\mathcal{A}_h^p((\boldsymbol{u}_{ph},\boldsymbol{w}_{ph}),(\boldsymbol{v},\boldsymbol{z}))+\mathcal{A}_h^f(\boldsymbol{\Sigma}_{fh},\boldsymbol{\tau})+\mathcal{B}^f(\boldsymbol{r}_{fh},\boldsymbol{\tau})-\mathcal{B}^f(\boldsymbol{\lambda},\dot{\boldsymbol{\Sigma}}_{fh})\\&+\mathcal{C}^{pf}((\dot{\boldsymbol{u}}_{ph},\dot{\boldsymbol{w}}_{ph}),\boldsymbol{\tau})-\mathcal{C}^{fp}(\dot{\boldsymbol{\Sigma}}_{fh},(\boldsymbol{v},\boldsymbol{z}))=\mathcal{F}(\boldsymbol{v},\boldsymbol{z},\boldsymbol{\tau}),\end{aligned}\tag{21}$$

with initial conditions $\boldsymbol{u}_{ph}(0)=\boldsymbol{u}_{0\,h}$, $\dot{\boldsymbol{u}}_{ph}(0)=\boldsymbol{v}_{0\,h}$, $\boldsymbol{w}_{ph}(0)=\boldsymbol{w}_{0\,h}$, $\dot{\boldsymbol{w}}_{ph}(0)=,\boldsymbol{z}_{0\,h}$ and $\boldsymbol{\Sigma}_{fh}(0)=\boldsymbol{0}$, where $\boldsymbol{u}_{0\,h},\boldsymbol{v}_{0\,h},\boldsymbol{w}_{0\,h}$, and $\boldsymbol{z}_{0\,h}$ are the $\boldsymbol{L}^2$-orthogonal projection of the initial data in (1). The bilinear form $\mathcal{A}_h^p(\cdot,\cdot)$ can be splitted as

$$\mathcal{A}_h^p((\boldsymbol{u},\boldsymbol{w}),(\boldsymbol{v},\boldsymbol{z})):=\mathcal{A}_h^e(\boldsymbol{u},\boldsymbol{v})+\mathcal{B}_h^p(\beta\boldsymbol{u}+\boldsymbol{w},\beta\boldsymbol{v}+\boldsymbol{z})\tag{22}$$

where for any $\boldsymbol{u},\boldsymbol{w},\boldsymbol{v},\boldsymbol{z}\in\boldsymbol{V}_h^p$, and for any $\boldsymbol{\Sigma},\boldsymbol{\tau}\in\boldsymbol{S}_h^f$ it holds

$$\begin{aligned}\mathcal{A}_h^e(\boldsymbol{u},\boldsymbol{v}):=&(\boldsymbol{\sigma}_{eh}(\boldsymbol{u}),\boldsymbol{\varepsilon}_h(\boldsymbol{v}))_{\Omega_p}-\langle\{\boldsymbol{\sigma}_{eh}(\boldsymbol{u})\},[[\boldsymbol{v}]]\rangle_{\mathcal{F}_h^p}\\&-\langle[[\boldsymbol{u}]],\{\boldsymbol{\sigma}_{eh}(\boldsymbol{v})\}\rangle_{\mathcal{F}_h^p}+\langle\chi_e[[\boldsymbol{u}]],[[\boldsymbol{v}]]\rangle_{\mathcal{F}_h^p},\end{aligned}\tag{23}$$

$$\begin{aligned}\mathcal{B}_h^p(\boldsymbol{w},\boldsymbol{z}):=&(m\nabla_h\cdot\boldsymbol{w},\nabla_h\cdot\boldsymbol{z})_{\Omega_p}-\langle\{m\nabla_h\cdot\boldsymbol{w}\},[[\boldsymbol{z}]]_{\boldsymbol{n}}\rangle_{\mathcal{F}_h^p}\\&-\langle[[\boldsymbol{w}]]_{\boldsymbol{n}},\{m\nabla_h\cdot\boldsymbol{z}\}\rangle_{\mathcal{F}_h^p}+\langle\chi_p[[\boldsymbol{w}]]_{\boldsymbol{n}},[[\boldsymbol{z}]]_{\boldsymbol{n}}\rangle_{\mathcal{F}_h^p},\end{aligned}\tag{24}$$

$$\begin{aligned}\mathcal{A}_h^f(\boldsymbol{\Sigma},\boldsymbol{\tau}):=&(\rho_f^{-1}\nabla_h\cdot\boldsymbol{\Sigma},\nabla_h\cdot\boldsymbol{\tau})_{\Omega_f}-\langle\{\rho_f^{-1}\nabla_h\cdot\boldsymbol{\Sigma}\},[[\boldsymbol{\tau}]]\rangle_{\mathcal{F}_h^f}\\&-\langle[[\boldsymbol{\Sigma}]],\{\rho_f^{-1}\nabla_h\cdot\boldsymbol{\tau}\}\rangle_{\mathcal{F}_h^f}+\langle\chi_f[[\boldsymbol{\Sigma}]],[[\boldsymbol{\tau}]]\rangle_{\mathcal{F}_h^f}.\end{aligned}\tag{25}$$

Finally, we define the penalization functions $\chi_e,\chi_p\in L^\infty(\Omega_p)$, and $\chi_f\in L^\infty(\Omega_f)$ appearing in (23),(24), and (25), respectively:

$$\chi_e|_F:=\begin{cases}c_1\max\limits_{K\in\{K^+,K^-\}}\overline{\mathbb{C}}_K\,p_{p,K}^2h_K^{-1} & \forall F\in\mathcal{F}_h^{p,i},\quad F\subseteq\partial K^+\cap\partial K^-,\\ \overline{\mathbb{C}}_K\,p_{p,K}^2h_K^{-1} & \forall F\in\mathcal{F}_h^{p,b},\quad F\subseteq\partial K,\end{cases}\tag{26}$$

$$\chi_p|_F:=\begin{cases}c_2\max\limits_{K\in\{K^+,K^-\}}\overline{m}_K\,p_{p,K}^2h_K^{-1} & \forall F\in\mathcal{F}_h^{p,i},\quad F\subseteq\partial K^+\cap\partial K^-,\\ \overline{m}_K\,p_{p,K}^2h_K^{-1} & \forall F\in\mathcal{F}_h^{p,b},\quad F\subseteq\partial K,\end{cases}\tag{27}$$

$$\chi_f|_F:=\begin{cases}c_3\max\limits_{K\in\{K^+,K^-\}}(\overline{\rho_f}_K)^{-1}p_{f,K}^2h_K^{-1} & \forall F\in F_h^{f,i},\quad F\subseteq\partial K^+\cap\partial K^-\\ (\overline{\rho_f}_K)^{-1}p_{f,K}^2h_K^{-1} & \forall F\in\mathcal{F}_h^{p,b},\quad F\subseteq\partial K,\end{cases}\tag{28}$$

with c_1, c_2, $c_3>0$ positive constants to be suitably chosen.

3.3 Stability and semi-discrete error analysis

To carry out the stability analysis of the semi-discrete problem (21), we introduce the energy norm defined for any $(\boldsymbol{u},\boldsymbol{w})\in C^1((0,T];\boldsymbol{V}_h^p\times\boldsymbol{V}_h^p)$, and $\boldsymbol{\Sigma}\in C^0((0,T];\boldsymbol{V}_h^f)$ as

$$\|(\boldsymbol{u},\boldsymbol{w},\boldsymbol{\Sigma})(t)\|_{\mathrm{E}}^2:=\|(\boldsymbol{u},\boldsymbol{w})(t)\|_{\mathrm{E}_p}^2+\|\boldsymbol{\Sigma}(t)\|_{\mathrm{E}_f}^2,\tag{29}$$

with

$$\begin{aligned}\|(\boldsymbol{u},\boldsymbol{w})(t)\|_{\mathrm{E}_p}^2:=&\|\dot{\boldsymbol{u}}(t)\|_{\Omega_p}^2+\|\dot{\boldsymbol{w}}(t)\|_{\Omega_p}^2+\|(\eta/k)^{\frac12}\boldsymbol{w}(t)\|_{\Omega_p}^2\\&+\|\gamma^{\frac12}\boldsymbol{w}\cdot\boldsymbol{n}_p(t)\|_{\Gamma_I}^2+\|\boldsymbol{u}\|_{\mathrm{dG,e}}^2+|(\beta\boldsymbol{u}+\boldsymbol{w})(t)|_{\mathrm{dG,p}}^2,\\\|\boldsymbol{\Sigma}(t)\|_{\mathrm{E}_f}^2:=&\|(1/2\mu_f)^{\frac12}\mathrm{dev}(\boldsymbol{\Sigma})(t)\|_{\Omega_f}^2+|\boldsymbol{\Sigma}(t)|_{dG,f}^2+\|\delta^{-\frac12}\boldsymbol{\Sigma}\boldsymbol{n}_p\wedge\boldsymbol{n}_p(t)\|_{\Gamma_I}^2,\end{aligned}$$

and where

$$\begin{aligned}\|\boldsymbol{v}\|_{\mathrm{dG,e}}^2:=&\|\mathbb{C}^{1/2}\boldsymbol{\varepsilon}_h(\boldsymbol{v})\|_{\Omega_p}^2+\|\chi_e^{1/2}[[\boldsymbol{v}]]\|_{\mathcal{F}_h^p\cup\mathcal{F}_h^{p,D}}^2 &&\forall\boldsymbol{v}\in\boldsymbol{V}_h^p,\\|\boldsymbol{z}|_{\mathrm{dG,p}}^2:=&\|m^{1/2}\nabla_h\cdot\boldsymbol{z}\|_{\Omega_p}^2+\|\chi_p^{1/2}[[\boldsymbol{z}]]_{\boldsymbol{n}}\|_{\mathcal{F}_h^p\cup\mathcal{F}_h^{p,D}}^2 &&\forall\boldsymbol{z}\in\boldsymbol{V}_h^p,\\|\boldsymbol{\sigma}|_{\mathrm{dG,\,f}}^2:=&\|(\rho_f)^{-\frac12}\nabla_h\cdot\boldsymbol{\sigma}\|_{\Omega_f}^2+\|\,\chi_f^{1/2}[[\boldsymbol{\sigma}]]\,\|_{\mathcal{F}_h^f\cup\mathcal{F}_h^{f,N}}^2 &&\forall\boldsymbol{\sigma}\in\boldsymbol{S}_h^f,\end{aligned}$$

with χ_e, χ_p, and χ_f defined as in (26), (27), and (28), respectively. For later use, we also define the following augmented norm or any $(\boldsymbol{u},\boldsymbol{w})\in C^1((0,T];\boldsymbol{H}^2(\mathcal{T}_h^p)\times\boldsymbol{H}^2(\mathcal{T}_h^p))$, and any $\boldsymbol{\Sigma}\in C^0((0,T];\mathbb{H}^2(\mathcal{T}_h^f))$ as

$$|||(\boldsymbol{u},\boldsymbol{w},\boldsymbol{\Sigma})|||_{\mathrm{E}}^2:=|||(\boldsymbol{u},\boldsymbol{w})(t)|||_{\mathrm{E}_p}^2+|||\boldsymbol{\Sigma}(t)|||_{\mathrm{E}_f}^2,$$

with

$$\begin{aligned}|||(\boldsymbol{u},\boldsymbol{w})(t)|||_{\mathrm{E}_p}^2:=&\|\dot{\boldsymbol{u}}(t)\|_{\Omega_p}^2+\|\dot{\boldsymbol{w}}(t)\|_{\Omega_p}^2+\|(\eta/k)^{\frac12}\boldsymbol{w}(t)\|_{\Omega_p}^2\\&+\|\gamma^{\frac12}\boldsymbol{w}\cdot\boldsymbol{n}_p(t)\|_{\Gamma_I}^2+|||\boldsymbol{u}(t)|||_{\mathrm{dG,e}}^2+|||(\beta\boldsymbol{u}+\boldsymbol{w})(t)|||_{\mathrm{dG,p}}^2,\\|||\boldsymbol{\Sigma}(t)|||_{\mathrm{E_f}}^2:=&\|(1/2\mu_f)^{\frac12}\mathrm{dev}(\boldsymbol{\Sigma})(t)\|_{\Omega_f}^2+|||\boldsymbol{\Sigma}(t)|||_{dG,f}^2+\|\delta^{-\frac12}\boldsymbol{\Sigma}\boldsymbol{n}_p\wedge\boldsymbol{n}_p(t)\|_{\Gamma_I}^2,\end{aligned}$$

and where

$$\begin{aligned}|||\boldsymbol{v}|||_{\mathrm{dG,e}}^2:=&\|\boldsymbol{v}\|_{\mathrm{dG,e}}^2+\|\chi_e^{-1/2}\{\mathbb{C}\boldsymbol{\varepsilon}_h(\boldsymbol{v})\}\|_{\mathcal{F}_h^p}^2 &&\forall\boldsymbol{v}\in\boldsymbol{H}^2(\mathcal{T}_h^p),\\|||\boldsymbol{z}|||_{\mathrm{dG,p}}^2:=&|\boldsymbol{z}|_{\mathrm{dG,p}}^2+\|\chi_p^{-1/2}\{m\nabla_h\cdot\boldsymbol{z}\}\|_{\mathcal{F}_h^p\cup\mathcal{F}_h^I}^2 &&\forall\boldsymbol{z}\in\boldsymbol{H}^2(\mathcal{T}_h^p),\\|||\boldsymbol{\sigma}|||_{\mathrm{dG,f}}^2:=&|\boldsymbol{\sigma}|_{\mathrm{dG,f}}^2+\|\chi_f^{-1/2}\{\boldsymbol{\nabla}_h\cdot\boldsymbol{\sigma}\}\|_{\mathcal{F}_h^f}^2 &&\forall\boldsymbol{\sigma}\in\mathbb{H}^2(\mathcal{T}_h^f).\end{aligned}$$

The following Lemma establishes the coercivity and boundedness of the discrete bilinear forms $\mathcal{A}_h^e$, $\mathcal{B}_h^p$, and $\mathcal{A}_h^f$ defined in (23),(24), and (25), respectively.

Lemma 3 Let Assumption 1 be satisfied. Then, it holds

$$\begin{aligned}
&\mathcal{A}_h^e(\boldsymbol{u},\boldsymbol{v}) \lesssim \|\boldsymbol{u}\|_{\mathrm{dG,e}}\|\boldsymbol{v}\|_{\mathrm{dG,e}} && \mathcal{A}_h^e(\boldsymbol{u},\boldsymbol{u}) \gtrsim \|\boldsymbol{u}\|^2_{\mathrm{dG,e}} \forall \boldsymbol{u},\boldsymbol{v}\in \boldsymbol{V}_h^p,\\
&\mathcal{B}_h^p(\boldsymbol{u},\boldsymbol{v}) \lesssim |\boldsymbol{u}|_{\mathrm{dG,p}}|\boldsymbol{v}|_{\mathrm{dG,p}} && \mathcal{B}_h^p(\boldsymbol{u},\boldsymbol{u}) \gtrsim |\boldsymbol{u}|^2_{\mathrm{dG,p}} \forall \boldsymbol{u},\boldsymbol{v}\in \boldsymbol{V}_h^p,\\
&\mathcal{A}_h^f(\boldsymbol{\sigma},\boldsymbol{\tau}) \lesssim |\boldsymbol{\sigma}_h|_{\mathrm{dG,f}}|\boldsymbol{\tau}_h|_{\mathrm{dG,f}} && \mathcal{A}_h^f(\boldsymbol{\sigma},\boldsymbol{\sigma}) \gtrsim |\boldsymbol{\sigma}_h|^2_{\mathrm{dG,f}} \forall \boldsymbol{\sigma},\boldsymbol{\tau}\in \boldsymbol{S}_h^f,\\
&\mathcal{A}_h^e(\boldsymbol{u},\boldsymbol{v}) \lesssim |||\boldsymbol{u}|||_{\mathrm{dG,e}}\|\boldsymbol{v}\|_{\mathrm{dG,e}} && \forall \boldsymbol{u}\in \boldsymbol{H}^2(\mathcal{T}_h^p) \forall \boldsymbol{v}\in \boldsymbol{V}_h^p,\\
&\mathcal{B}_h^p(\boldsymbol{w},\boldsymbol{z}) \lesssim |||\boldsymbol{w}|||_{\mathrm{dG,p}}|\boldsymbol{z}|_{\mathrm{dG,p}} && \forall \boldsymbol{w}\in \boldsymbol{H}^2(\mathcal{T}_h^p) \forall \boldsymbol{z}\in \boldsymbol{V}_h^p,\\
&\mathcal{A}_h^f(\boldsymbol{\sigma},\boldsymbol{\tau}) \lesssim |||\boldsymbol{\sigma}|||_{\mathrm{dG,f}}|\boldsymbol{\tau}|_{\mathrm{dG,f}} && \forall \boldsymbol{\sigma}\in \mathbb{H}^2(\mathcal{T}_h^f) \forall \boldsymbol{\tau}\in \boldsymbol{S}_h^f.
\end{aligned}$$

The coercivity bounds hold provided that the stability parameters c_1, c_2, and c_3 in (26), (27), and (28), respectively, are chosen sufficiently large.

Proof The proof is based on employing the same arguments as in [26, Lemma A.3] and in [27, Lemma 3]. □

Theorem 2 For any time $t\in(0,T]$ let $(\boldsymbol{u}_{ph},\boldsymbol{w}_{ph},\boldsymbol{\Sigma}_{fh},\boldsymbol{r}_{fh})(t)\in \boldsymbol{V}_h$ the solution to problem (21). Then, it holds

$$\sup_{t\in(0,T]} \|(\boldsymbol{u}_{ph},\boldsymbol{w}_{ph},\boldsymbol{\Sigma}_{fh})(t)\|_{\mathrm{E}} \lesssim \mathcal{G}_{0h} + \int_0^T \mathcal{N}(\boldsymbol{f}_p,\boldsymbol{g}_p,\boldsymbol{F}_f,\boldsymbol{G}_f)(s)\,ds$$

where

$$\mathcal{G}_{0h}^2 = \|(\boldsymbol{u}_{ph},\boldsymbol{w}_{ph},\boldsymbol{\Sigma}_{fh})(0)\|^2_{\mathcal{E}} + \sup_{t\in[0,T]}\left(\|\boldsymbol{F}_f(t)\|^2_{\Omega_f} + \|\boldsymbol{G}_f(t)\|^2_{\Gamma_I\cup\Gamma_f^D}\right), \tag{30}$$

and $\mathcal{N}$ is defined as in (18).

Proof The assertion follows the lines for the proof of Theorem 1 and uses the results in Lemma 3. □

3.4 Error analysis

In this section, we prove an a-priori error estimate in the energy norm (29) for the semi-discrete problem (21). We start by introducing the following notation for any time $t\in(0,T]$,

$$\begin{aligned}
\boldsymbol{e}^u(t) &:= (\boldsymbol{u}_p - \boldsymbol{u}_{ph})(t) = (\boldsymbol{u}_p - \boldsymbol{u}_{pI})(t) + (\boldsymbol{u}_{pI} - \boldsymbol{u}_{ph})(t) = \boldsymbol{e}_I^u(t) - \boldsymbol{e}_h^u(t),\\
\boldsymbol{e}^w(t) &:= (\boldsymbol{w}_p - \boldsymbol{w}_{ph})(t) = (\boldsymbol{w}_p - \boldsymbol{w}_{pI})(t) + (\boldsymbol{w}_{pI} - \boldsymbol{w}_{ph})(t) = \boldsymbol{e}_I^w(t) - \boldsymbol{e}_h^w(t),\\
\boldsymbol{e}^\Sigma(t) &:= (\boldsymbol{\Sigma}_f - \boldsymbol{\Sigma}_{fh})(t) = (\boldsymbol{\Sigma}_f - \boldsymbol{\Sigma}_{fI})(t) + (\boldsymbol{\Sigma}_{fI} - \boldsymbol{\Sigma}_{fh})(t) = \boldsymbol{e}_I^\Sigma(t) - \boldsymbol{e}_h^\Sigma(t),\\
\boldsymbol{e}^r(t) &:= (\boldsymbol{r}_f - \boldsymbol{r}_{fh})(t) = (\boldsymbol{r}_f - \boldsymbol{r}_{fI})(t) + (\boldsymbol{r}_{fI} - \boldsymbol{r}_{fh})(t) = \boldsymbol{e}_I^r(t) - \boldsymbol{e}_h^r(t),
\end{aligned}$$

being $\boldsymbol{u}_{pI}, \boldsymbol{w}_{pI}, \boldsymbol{\Sigma}_{fI}$, and $\boldsymbol{r}_{fI}$ suitable interpolant functions that are going to be defined in Lemma 4. We observe that (21) is *strongly consistent* in the sense that the error equation reads as follows for any $(\boldsymbol{v},\boldsymbol{z},\boldsymbol{\tau},\boldsymbol{\lambda})\in \boldsymbol{V}_h$:

$$\begin{aligned}
&\mathcal{M}^p((\ddot{\boldsymbol{e}}^u,\ddot{\boldsymbol{e}}^w),(\boldsymbol{v},\boldsymbol{z})) + \mathcal{M}^f(\dot{\boldsymbol{e}}^\Sigma,\boldsymbol{\tau}) + \mathcal{D}^p(\dot{\boldsymbol{e}}^w,\boldsymbol{z}) + \mathcal{D}^f(\dot{\boldsymbol{e}}^\Sigma,\boldsymbol{\tau}) + \mathcal{A}_h^p((\boldsymbol{e}^u,\boldsymbol{e}^w),(\boldsymbol{v},\boldsymbol{z}))\\
&\quad + \mathcal{A}_h^f(\boldsymbol{e}^\Sigma,\boldsymbol{\tau}) + \mathcal{B}^f(\boldsymbol{e}^r,\boldsymbol{\tau}) - \mathcal{B}^f(\boldsymbol{\lambda},\dot{\boldsymbol{e}}^\Sigma) + \mathcal{C}^{pf}((\dot{\boldsymbol{e}}^u,\dot{\boldsymbol{e}}^w),\boldsymbol{\tau}) - \mathcal{C}^{fp}(\dot{\boldsymbol{e}}^\Sigma,(\boldsymbol{v},\boldsymbol{z})) = 0.
\end{aligned} \tag{31}$$

For an open bounded polytopic domain $\Upsilon\subset\mathbb{R}^d$ and a generic polytopic mesh $\mathcal{T}_h$ over Υ satisfying Assumption 2, as in [50], we can introduce the Stein extension operator $\tilde{\mathcal{E}}: H^m(\kappa)\to H^m(\mathbb{R}^d)$ [52], for any $\kappa\in\mathcal{T}_h$ and $m\in\mathbb{N}_0$, such that $\tilde{\mathcal{E}}v|_\kappa = v$ and $\|\tilde{\mathcal{E}}v\|_{m,\mathbb{R}^d}\lesssim\|v\|_{m,\kappa}$. The corresponding vector-valued and tensor-valued versions mapping $\boldsymbol{H}^m(\kappa)$ and $\mathbb{H}^m(\kappa)$ onto $\boldsymbol{H}^m(\mathbb{R}^d)$ and $\mathbb{H}^m(\mathbb{R}^d)$ act component-wise and are denoted in the same way. In what follows, for any $\kappa\in\mathcal{T}_h$, we will denote by $\mathcal{K}_\kappa$ the simplex belonging to the covering $\mathcal{T}_\S$ such that $\kappa\subset\mathcal{K}_\kappa$, cf. Assumption 2.

The next Lemma provides the interpolation bounds that are instrumental for the derivation of the a-priori error estimate.

Lemma 4 For any $(\boldsymbol{u},\boldsymbol{w})\in C^1([0,T];\boldsymbol{H}^m(\mathcal{T}_h^p)\times\boldsymbol{H}^\ell(\mathcal{T}_h^p))$, with $m,\ell\geq 2$, there exists $(\boldsymbol{u}_I,\boldsymbol{w}_I)\in C^1([0,T];\boldsymbol{V}_h^p\times\boldsymbol{V}_h^p)$ s.t.:

$$\begin{aligned}
|||(\boldsymbol{u}-\boldsymbol{u}_I,\boldsymbol{w}-\boldsymbol{w}_I)|||^2_{\mathrm{E_p}} &\lesssim \sum_{\kappa\in\mathcal{T}_h^p}\frac{h_\kappa^{2(s_\kappa-1)}}{p_{p,\kappa}^{2m-3}}\left(\|\widetilde{\mathcal{E}}\dot{\boldsymbol{u}}\|^2_{m,\mathcal{K}_\kappa} + \|\widetilde{\mathcal{E}}\boldsymbol{u}\|^2_{m,\mathcal{K}_\kappa}\right)\\
&\quad + \sum_{\kappa\in\mathcal{T}_h^p}\frac{h_\kappa^{2(r_\kappa-1)}}{p_{p,\kappa}^{2\ell-3}}\left(\|\widetilde{\mathcal{E}}\dot{\boldsymbol{w}}\|^2_{\ell,\mathcal{K}_\kappa} + \|\widetilde{\mathcal{E}}\boldsymbol{w}\|^2_{\ell,\mathcal{K}_\kappa}\right).
\end{aligned} \tag{32}$$

where $s_\kappa = \min(m, p_{p,\kappa}+1)$, and $r_\kappa = \min(\ell, p_{p,\kappa}+1)$. Also, for any $\boldsymbol{\Sigma}\in C^0([0,T];\mathbb{H}^n(\mathcal{T}_h^f))$, with $n\geq 2$, there exists $\boldsymbol{\Sigma}_I\in C^0([0,T];\boldsymbol{S}_h^f)$ s.t.:

$$|||\boldsymbol{\Sigma}-\boldsymbol{\Sigma}_I|||^2_{\mathrm{E_f}} \lesssim \sum_{\kappa\in\mathcal{T}_h^f}\frac{h_\kappa^{2(q_\kappa-1)}}{p_{f,\kappa}^{2n-3}}\|\widetilde{\mathcal{E}}\boldsymbol{\Sigma}\|^2_{n,\mathcal{K}_\kappa}, \tag{33}$$

where $q_\kappa = \min(n, p_{f,\kappa}+1)$. Moreover, for any $\boldsymbol{r}\in C^0([0,T];\boldsymbol{H}^\nu(\mathcal{T}_h^f))$, with $\nu\geq 2$, there exists $\boldsymbol{r}_I\in C^0([0,T];\boldsymbol{\Lambda}_h^f)$ s.t.:

$$\|\boldsymbol{r}-\boldsymbol{r}_I\|^2_{\Omega_f} \lesssim \sum_{\kappa\in\mathcal{T}_h^f}\frac{h_\kappa^{2\zeta_\kappa}}{(p_{f,\kappa}-1)^{2\nu}}\|\widetilde{\mathcal{E}}\boldsymbol{r}\|^2_{\nu,\mathcal{K}_\kappa}, \tag{34}$$

where $\zeta_\kappa = \min(\nu, p_{f,\kappa})$.

Proof We prove (32) by combining the results in [29, Lemma 33] with the ones in [26, Lemma 4.2] while we obtain (33) by combining again the results in [29, Lemma 33] with the ones in [27, Lemma 4.1]. □

In addition to the continuity and coercivity results of Lemma 3, the a-priori error analysis requires an inf-sup condition for the constraint form $\mathcal{B}^f(\cdot,\cdot)$, as follows:

Assumption 3 There exist a constant $\beta_h^f > 0$ such that the following inequality holds:

$$\sup_{\boldsymbol{\tau}\in\boldsymbol{S}_h^f\setminus\{\mathbf{0}\}} \frac{\mathcal{B}^f(\boldsymbol{\lambda}_h,\boldsymbol{\tau})}{\|\boldsymbol{\tau}\|_{\mathrm{E}_f} + \|\ \chi_f^{1/2}[[\boldsymbol{\sigma}]]\ \|^2_{\mathcal{F}_h^I}} \geq \beta_h^f \|\boldsymbol{\lambda}_h\|_{\Omega_f}, \qquad \forall\, \boldsymbol{\lambda}_h \in \boldsymbol{\Lambda}_h^f. \tag{35}$$

Although the previous result is not available for polygonal meshes (and will be the subject of future work), it can be proven for matching simplicial meshes (that coincide with their covering $\mathcal{T}_{\S}$ defined in Assumption 2). In this case, the proof of the inf-sup inequality (35) is based on [44], with modifications to account for the interface terms in the norm $\|\boldsymbol{\tau}\|_{\mathrm{E}_f}$ and in the additional term in the denominator, and it is reported in Appendix A.

Under the previous assumption, we can establish the instrumental result:

Lemma 5 Let Assumption 3 be verified. Then, the following holds:

$$\beta_h^f \|\boldsymbol{e}_h^r\|_{\Omega_f} \lesssim \|\dot{\boldsymbol{e}}_h^\Sigma\|_{\mathrm{E}_\ell} + \|\boldsymbol{e}_h^\Sigma\|_{\mathrm{E}_\ell} + \|(\dot{\boldsymbol{e}}_h^u, \dot{\boldsymbol{e}}_h^w)\|_{\mathrm{E}_p} + |||\dot{\boldsymbol{e}}_I^\Sigma|||_{\mathrm{E}_\ell} + |||\boldsymbol{e}_I^\Sigma|||_{\mathrm{E}_\ell} + \|(\dot{\boldsymbol{e}}_I^r, \dot{\boldsymbol{e}}_I^w)\|_{\mathrm{E}_p} + \|\boldsymbol{e}_I^r\|_{\Omega_f} \tag{36}$$

Proof To prove (36), we start from the error equation (31) with $\boldsymbol{v} = \mathbf{0}, \boldsymbol{z} = \mathbf{0}, \boldsymbol{\lambda} = \mathbf{0}$, and a generic $\boldsymbol{\tau} \in \boldsymbol{S}_h^f$. Rearranging the terms to isolate $\mathcal{B}^f(\boldsymbol{e}_h^r, \boldsymbol{\tau})$ on one side of the equality, using the continuity results of Lemmas 2 and 3 and the trace-inverse inequality (20) on the interface term $\mathcal{C}^{pf}$, we obtain the following:

$$\begin{aligned}\mathcal{B}^f(\boldsymbol{e}_h^r,\boldsymbol{\tau}) = \mathcal{M}^f(\dot{\boldsymbol{e}}^\Sigma,\boldsymbol{\tau}) + \mathcal{D}^f(\dot{\boldsymbol{e}}^\Sigma,\boldsymbol{\tau}) + \mathcal{A}_h^f(\boldsymbol{e}^\Sigma,\boldsymbol{\tau}) + \mathcal{C}^{pf}((\dot{\boldsymbol{e}}^u,\dot{\boldsymbol{e}}^w),\boldsymbol{\tau}) + \mathcal{B}^f(\boldsymbol{e}_I^r,\boldsymbol{\tau}) \lesssim \\ (\|\dot{\boldsymbol{e}}_h^\Sigma\|_{\mathrm{E}_f} + \|\boldsymbol{e}_h^\Sigma\|_{\mathrm{E}_f})\|\boldsymbol{\tau}\|_{\mathrm{E}_f} + \|\ \chi_f^{1/2}\boldsymbol{\tau}\boldsymbol{n}_p\|^2_{\mathcal{F}_h^I}(\|\dot{\boldsymbol{e}}_h^u\|_{\mathrm{E}_p} \\ + \|\dot{\boldsymbol{e}}_h^w\|_{\mathrm{E}_p} + \|\dot{\boldsymbol{e}}_I^u\|_{\mathrm{E}_p} + \|\dot{\boldsymbol{e}}_I^w\|_{\mathrm{E}_p}) + (|||\dot{\boldsymbol{e}}_I^\Sigma|||_{\mathrm{E}_f} + |||\boldsymbol{e}_h^\Sigma|||_{\mathrm{E}_f} + \|\boldsymbol{e}_I^r\|_{\Omega_f})\|\boldsymbol{\tau}\|_{\mathrm{E}_f}.\end{aligned}$$

Taking the supremum over $\boldsymbol{\tau} \in \boldsymbol{S}_h^f \setminus \{\mathbf{0}\}$ and using the inf-sup condition (35) completes the proof. □

We are now ready to state the main result of this section.

Theorem 3 (A-priori error estimates) Let Assumption 1 and 2, and the hypothesis of Theorem 1 hold and let the exact solution $(\boldsymbol{u}_p, \boldsymbol{w}_p, \boldsymbol{\Sigma}_f, \boldsymbol{r}_f)$ of problem (9) be such that

$$\begin{aligned}&(\boldsymbol{u}_p, \boldsymbol{w}_p) \in C^2((0,T];\boldsymbol{H}^m(\mathcal{T}_h^p)\times\boldsymbol{H}^\ell(\mathcal{T}_h^p)) \cap C^1([0,T];\boldsymbol{H}_0^1(\Omega_p)\times\boldsymbol{H}_{0,\Gamma_p^D}(\mathrm{div},\Omega_p)),\\ &\boldsymbol{\Sigma}_f \in C^1((0,T];\mathbb{H}^n(\mathcal{T}_h^f)) \cap C^0([0,T];\mathbb{H}_{0,\Gamma_p^N}(\mathrm{div},\Omega_f)),\ \textit{and}\\ &\boldsymbol{r}_f \in C^0((0,T];\ H^\nu(\mathcal{T}_h^f)^{d^*}),\end{aligned}$$

with integers $m, \ell, n \geq 2$ and $\nu \geq 1$ and let $(\boldsymbol{u}_{ph}, \boldsymbol{w}_{ph}, \boldsymbol{\Sigma}_{fh}, \boldsymbol{r}_{fh})$ such that

$$(\boldsymbol{u}_{ph}, \boldsymbol{w}_{ph}) \in C^2([0,T];\boldsymbol{V}_h^p\times\boldsymbol{V}_h^p),\ \boldsymbol{\Sigma}_{fh} \in C^1([0,T];\boldsymbol{S}_h^f),\ \textit{and}\ \boldsymbol{r}_{fh} \in C^0([0,T];\ \boldsymbol{\Lambda}_h^f),$$

be the solution of the semi-discrete problem (21), with sufficiently large penalty parameters c_1, c_2, and c_3. Then, for any $t \in (0,t]$, the discretization error $\boldsymbol{E}(t) = (\boldsymbol{e}^u, \boldsymbol{e}^w, \boldsymbol{e}^\Sigma)(t)$ satisfies

$$\begin{aligned}\sup_{t\in(0,T]} \|\boldsymbol{E}(t)\|_{\mathrm{E}} \lesssim &\sum_{\kappa\in\mathcal{T}_h^p}\left(\frac{h_\kappa^{s_\kappa-1}}{p_{p,\kappa}^{m-3/2}}\Theta_{\boldsymbol{u}} + \frac{h_\kappa^{r_\kappa-1}}{p_{p,\kappa}^{\ell-3/2}}\Theta_{\boldsymbol{w}}\right)\\ &+ \sum_{\kappa\in\mathcal{T}_h^f}\left(\frac{h_\kappa^{q_\kappa-1}}{p_{f,\kappa}^{n-3/2}}\Theta_{\boldsymbol{\Sigma}} + \frac{h_\kappa^{\zeta_\kappa}}{(p_{f,\kappa}-1)^\nu}\Theta_{\boldsymbol{r}}\right)\end{aligned}$$

where

$$\begin{aligned}\Theta_{\boldsymbol{u}} &:= \sup_{t\in(0,T]}\left(\|\widetilde{\mathcal{E}}\boldsymbol{u}(t)\|_{m,\mathcal{K}_\kappa} + \|\widetilde{\mathcal{E}}\boldsymbol{u}(t)\|_{m,\mathcal{K}_\kappa}\right) + \int_0^T\left(\|\widetilde{\mathcal{E}}\dot{\boldsymbol{u}}(s)\|_{m,\mathcal{K}_\kappa} + \|\widetilde{\mathcal{E}}\dot{\boldsymbol{u}}(s)\|_{m,\mathcal{K}_\kappa}\right)ds,\\ \Theta_{\boldsymbol{w}} &:= \sup_{t\in(0,T]}\left(\|\widetilde{\mathcal{E}}\dot{\boldsymbol{w}}(t)\|_{m,\mathcal{K}_\kappa} + \|\widetilde{\mathcal{E}}\boldsymbol{w}(t)\|_{m,\mathcal{K}_\kappa}\right) + \int_0^T\left(\|\widetilde{\mathcal{E}}\dot{\boldsymbol{w}}(s)\|_{m,\mathcal{K}_\kappa} + \|\widetilde{\mathcal{E}}\dot{\boldsymbol{w}}(s)\|_{m,\mathcal{K}_\kappa}\right)ds,\\ \Theta_{\boldsymbol{\Sigma}} &:= \sup_{t\in(0,T]}\|\widetilde{\mathcal{E}}\boldsymbol{\Sigma}(t)\|_{n,\mathcal{K}_\kappa} + \int_0^T\|\widetilde{\mathcal{E}}\dot{\boldsymbol{\Sigma}}(s)\|_{n,\mathcal{K}_\kappa}ds,\\ \Theta_{\boldsymbol{r}} &:= \int_0^T\|\widetilde{\mathcal{E}}\boldsymbol{r}(s)\|_{\nu,\mathcal{K}_\kappa}ds,\end{aligned}$$

and where $s_\kappa = \min(m, p_{p,\kappa}+1), r_\kappa = \min(\ell, p_{p,\kappa}+1)$, $q_\kappa = \min(n, p_{f,\kappa}+1)$, and $\zeta_\kappa = \min(\nu, p_{f,\kappa})$ for any $\kappa \in \mathcal{T}_h$. Here the hidden constant depends on the material properties but is independent of the discretization parameters.

Proof We consider equation (31) for $\boldsymbol{v} = \dot{\boldsymbol{e}}_h^u, \boldsymbol{z} = \dot{\boldsymbol{e}}_h^w, \boldsymbol{\tau} = \dot{\boldsymbol{e}}_h^\Sigma$, and $\boldsymbol{\lambda} = \boldsymbol{e}_h^r$ to get

$$\begin{aligned}L_1 :=& \mathcal{M}^p((\ddot{\boldsymbol{e}}_h^u,\ddot{\boldsymbol{e}}_h^w),(\dot{\boldsymbol{e}}_h^u,\dot{\boldsymbol{e}}_h^w)) + \mathcal{D}^p(\dot{\boldsymbol{e}}_h^w,\dot{\boldsymbol{e}}_h^w) + \mathcal{A}_h^p((\boldsymbol{e}_h^u,\boldsymbol{e}_h^w),(\dot{\boldsymbol{e}}_h^u,\dot{\boldsymbol{e}}_h^w))\\ &+ \mathcal{M}^f(\dot{\boldsymbol{e}}_h^\Sigma,\dot{\boldsymbol{e}}_h^\Sigma) + \mathcal{D}^f(\dot{\boldsymbol{e}}_h^\Sigma,\dot{\boldsymbol{e}}_h^\Sigma) + \mathcal{A}_h^f(\boldsymbol{e}_h^\Sigma,\dot{\boldsymbol{e}}_h^\Sigma) = \mathcal{M}^p((\ddot{\boldsymbol{e}}_I^w,\ddot{\boldsymbol{e}}_I^w),(\dot{\boldsymbol{e}}_h^u,\dot{\boldsymbol{e}}_h^w)) + \mathcal{D}^p(\dot{\boldsymbol{e}}_I^w,\dot{\boldsymbol{e}}_I^w) + \mathcal{A}_h^p((\boldsymbol{e}_I^u,\boldsymbol{e}_I^w),(\dot{\boldsymbol{e}}_h^u,\dot{\boldsymbol{e}}_h^w))\\ &+ \mathcal{M}^f(\dot{\boldsymbol{e}}_I^\Sigma,\dot{\boldsymbol{e}}_h^\Sigma) + \mathcal{D}^f(\dot{\boldsymbol{e}}_I^\Sigma,\dot{\boldsymbol{e}}_h^\Sigma) + \mathcal{A}_h^f(\dot{\boldsymbol{e}}_I^\Sigma,\dot{\boldsymbol{e}}_h^\Sigma) + \mathcal{B}^f(\boldsymbol{e}_I^r,\dot{\boldsymbol{e}}_h^\Sigma) - \mathcal{B}^f(\boldsymbol{e}_h^r,\dot{\boldsymbol{e}}_I^\Sigma) + \mathcal{C}^{pf}((\dot{\boldsymbol{e}}_I^u,\dot{\boldsymbol{e}}_I^w),\dot{\boldsymbol{e}}_h^\Sigma)\\ &- \mathcal{C}^{fp}(\dot{\boldsymbol{e}}_I^\Sigma,(\dot{\boldsymbol{e}}_h^u,\dot{\boldsymbol{e}}_h^w)) =: L_2.\end{aligned}$$

By integrating L_1 and L_2 with respect to time in $(0, t)$ we obtain

$$\begin{aligned}\int_0^t L_1\,ds =& \frac{1}{2}\mathcal{M}^p((\dot{\boldsymbol{e}}_h^u,\dot{\boldsymbol{e}}_h^w),(\dot{\boldsymbol{e}}_h^u,\dot{\boldsymbol{e}}_h^w))\\ &+ \int_0^t\mathcal{D}^p(\dot{\boldsymbol{e}}_h^w,\dot{\boldsymbol{e}}_h^w)\,ds + \frac{1}{2}\mathcal{A}_h^p((\boldsymbol{e}_h^u,\boldsymbol{e}_h^w),(\boldsymbol{e}_h^u,\boldsymbol{e}_h^w))\\ &+ \int_0^t\mathcal{M}^f(\dot{\boldsymbol{e}}_h^\Sigma,\dot{\boldsymbol{e}}_h^\Sigma)\,ds + \int_0^t\mathcal{D}^f(\dot{\boldsymbol{e}}_h^\Sigma,\dot{\boldsymbol{e}}_h^\Sigma)\,ds + \frac{1}{2}\mathcal{A}_h^f(\boldsymbol{e}_h^\Sigma,\boldsymbol{e}_h^\Sigma),\end{aligned} \tag{37}$$

since $\boldsymbol{e}_h^u(0) = \boldsymbol{e}_h^w(0) = \dot{\boldsymbol{e}}_h^u(0) = \dot{\boldsymbol{e}}_h^w(0) = \boldsymbol{e}_h^\Sigma(0) = \mathbf{0}$ and

$$\begin{aligned}\int_0^t L_2\,ds = &\int_0^t\overbrace{\left(\mathcal{M}^p((\ddot{\boldsymbol{e}}_I^u,\ddot{\boldsymbol{e}}_I^w),(\dot{\boldsymbol{e}}_h^u,\dot{\boldsymbol{e}}_h^w)) + \mathcal{D}^p(\dot{\boldsymbol{e}}_I^w,\dot{\boldsymbol{e}}_h^w) - \mathcal{A}_h^p((\dot{\boldsymbol{e}}_I^u,\dot{\boldsymbol{e}}_I^w),(\boldsymbol{e}_h^u,\boldsymbol{e}_h^w))\right)}^{Y_1(s)}ds\\ &+ \overbrace{\mathcal{A}_h^p((\boldsymbol{e}_I^u,\boldsymbol{e}_I^w),(\boldsymbol{e}_h^u,\boldsymbol{e}_h^w))}^{Y_2}\\ &+ \int_0^t\overbrace{\left(\mathcal{M}^f(\dot{\boldsymbol{e}}_I^\Sigma,\dot{\boldsymbol{e}}_h^\Sigma) + \mathcal{D}^f(\dot{\boldsymbol{e}}_I^\Sigma,\dot{\boldsymbol{e}}_h^\Sigma) - \mathcal{A}_h^f(\dot{\boldsymbol{e}}_I^\Sigma,\boldsymbol{e}_h^\Sigma)\right)}^{Y_3(s)}ds + \overbrace{\mathcal{A}_h^f(\boldsymbol{e}_I^\Sigma,\boldsymbol{e}_h^\Sigma)}^{Y_4}\\ &+ \int_0^t\overbrace{\left(\mathcal{B}^f(\boldsymbol{e}_I^r,\dot{\boldsymbol{e}}_h^\Sigma) - \mathcal{B}^f(\boldsymbol{e}_h^r,\dot{\boldsymbol{e}}_I^\Sigma)\right)}^{Y_5(s)}ds + \int_0^t\left(\overbrace{\mathcal{C}^{pf}((\dot{\boldsymbol{e}}_I^u,\dot{\boldsymbol{e}}_I^w),\dot{\boldsymbol{e}}_h^\Sigma)}^{Y_6(s)} - \overbrace{\mathcal{C}^{fp}(\dot{\boldsymbol{e}}_I^\Sigma,(\dot{\boldsymbol{e}}_h^u,\dot{\boldsymbol{e}}_h^w))}^{Y_7(s)}\right)ds,\end{aligned}$$

respectively. Next, we treat separately the terms Y_i, $i = 1, \dots, 7$ as follows. For positive ϵ_i, $i = 1, \dots, 4$, we employ the Cauchy-Schwarz and Young inequalities as follows

$$\begin{aligned}\int_0^t Y_1(s)\,ds + Y_2 \lesssim \int_0^t |||(\dot{e}_I^u, \dot{e}_I^w)|||_{\mathrm{E_p}} \|(e_h^u, e_h^w)\|_{\mathrm{E_p}}\,ds \\ + \frac{1}{2\epsilon_1}\int_0^t \mathcal{D}^p(\dot{e}_I^w, \dot{e}_I^w)\,ds + \frac{\epsilon_1}{2}\int_0^t \mathcal{D}^p(\dot{e}_h^w, \dot{e}_h^w)\,ds \\ + \frac{1}{2\epsilon_2}\mathcal{A}_h^p((e_I^u, e_I^w), (e_I^u, e_I^w)) + \frac{\epsilon_2}{2}\mathcal{A}_h^p((e_h^u, e_h^w), (e_h^u, e_h^w)),\end{aligned} \tag{38}$$

and

$$\begin{aligned}\int_0^t Y_3(s)\,ds + Y_4 \lesssim \frac{1}{2\epsilon_3}\int_0^t \Big(\mathcal{M}^f(\dot{e}_I^\Sigma, \dot{e}_I^\Sigma) + \mathcal{D}^f(\dot{e}_I^\Sigma, \dot{e}_I^\Sigma)\Big)\,ds \\ + \frac{\epsilon_3}{2}\int_0^t \Big(\mathcal{M}^f(\dot{e}_h^\Sigma, \dot{e}_h^\Sigma) + \mathcal{D}^f(\dot{e}_h^\Sigma, \dot{e}_h^\Sigma)\Big)\,ds + \int_0^t |||\dot{e}_I^\Sigma|||_{\mathrm{E_f}} \|e_h^\Sigma\|_{\mathrm{E_f}}\,ds \\ + \frac{1}{2\epsilon_4}\mathcal{A}_h^f(e_I^\Sigma, e_I^\Sigma) + \frac{\epsilon_4}{2}\mathcal{A}_h^f(e_h^\Sigma, e_h^\Sigma).\end{aligned} \tag{39}$$

For Y_5, we employ the Cauchy-Schwarz and Young inequalities and then estimate (36) of Lemma 5 to obtain, for positive ϵ_5, ϵ_6,

$$\begin{aligned}\int_0^t Y_5(s)\,ds &\lesssim \int_0^t \frac{1}{2\epsilon_5}\|e_I^r\|_{\Omega_f}^2 + \int_0^t \frac{\epsilon_5}{2}\|\dot{e}_h^\Sigma\|_{\Omega_f}^2 + \int_0^t \frac{1}{2\epsilon_6}\|\dot{e}_I^\Sigma\|_{\Omega_f}^2 + \int_0^t \frac{\epsilon_6}{2}\|e_h^r\|_{\Omega_f}^2 \\ &\lesssim \int_0^t \frac{1}{2\epsilon_5}\|e_I^r\|_{\Omega_f}^2 + \int_0^t \frac{1}{2\epsilon_6}\|\dot{e}_I^\Sigma\|_{\Omega_f}^2 + \int_0^t \left(\frac{\epsilon_5}{2} + \frac{\epsilon_6}{2(\beta_h^f)^2}\right)\|\dot{e}_h^\Sigma\|_{\mathrm{E_f}}^2 \\ &\quad + \int_0^t \frac{\epsilon_6}{2(\beta_h^f)^2}\|e_h^\Sigma\|_{\mathrm{E_f}}^2 + \int_0^t \frac{\epsilon_6}{2(\beta_h^f)^2}\|(\dot{e}_h^u, \dot{e}_h^w)\|_{\mathrm{E_p}}^2 =: \mathcal{J}_{\mathcal{B}}^t.\end{aligned} \tag{40}$$

Finally, for the coupling terms in $\mathcal{C}^{fp}(\cdot)$ we use the inverse inequality (20) together with Assumption 1 to get

$$\begin{aligned}\int_0^t Y_7(s)\,ds &= \int_0^t \Big(< \dot{e}_I^\Sigma \boldsymbol{n}_p \cdot \boldsymbol{n}_p, (\alpha \dot{e}_h^u + \dot{e}_h^w) \cdot \boldsymbol{n}_p >_{\Gamma_I} + < e_I^\Sigma \boldsymbol{n}_p \wedge \boldsymbol{n}_p, \dot{e}_h^u \wedge \boldsymbol{n}_p >_{\Gamma_I} \Big)\,ds \\ &\lesssim \int_0^t \sum_{\kappa_p \in \mathcal{T}_{h,I}^p, \kappa_f \in \mathcal{T}_{h,I}^f} \|\dot{e}_I^\Sigma\|_{\partial\kappa_f}\Big(\|\dot{e}_h^u\|_{\partial\kappa_p} + \|\dot{e}_h^w\|_{\partial\kappa_p}\Big)\,ds \\ &\lesssim \int_0^t \Big(\sum_{\kappa \in \mathcal{T}_{h,I}^f} p_{f,\kappa} h_\kappa^{-1/2} \|\dot{e}_I^\Sigma\|_{\partial\kappa}\Big)\Big(\|\dot{e}_h^u\|_{\Omega_p} + \|\dot{e}_h^w\|_{\Omega_p}\Big)\,ds \\ &=: \int_0^t \mathcal{I}_h^f(\dot{e}_I^\Sigma)\Big(\|\dot{e}_h^u\|_{\Omega_p} + \|\dot{e}_h^w\|_{\Omega_p}\Big)\,ds,\end{aligned} \tag{41}$$

being $\mathcal{T}_{h,I}^p$ and $\mathcal{T}_{h,I}^f$ the sets of mesh elements sharing an edge with Γ_I. For Y_6, we use the integration by parts formula and we reason as before

$$\begin{aligned}\int_0^t Y_6(s)\,ds &= \mathcal{C}^{pf}((\dot{e}_I^u, \dot{e}_I^w), e_h^\Sigma) - \int_0^t \mathcal{C}^{pf}((\ddot{e}_I^u, \ddot{e}_I^w), e_h^\Sigma)\,ds \\ &\lesssim \sum_{\kappa \in \mathcal{T}_{h,p}^I} p_{p,\kappa} h_\kappa^{-1/2}\Big(\|\dot{e}_I^u\|_{\partial\kappa} + \|\dot{e}_I^w\|_{\partial\kappa}\Big)\|e_h^\Sigma\|_{\mathrm{E_f}} \\ &\quad + \int_0^t \sum_{\kappa \in \mathcal{T}_{h,p}^I} p_{p,\kappa} h_\kappa^{-1/2}\Big(\|\ddot{e}_I^u\|_{\partial\kappa} + \|\ddot{e}_I^w\|_{\partial\kappa}\Big)\|e_h^\Sigma\|_{\mathrm{E_f}}\,ds \\ &=: \mathcal{I}_h^p(\dot{e}_I^u, \dot{e}_I^w)\|e_h^\Sigma\|_{\mathrm{E_f}} + \int_0^t \mathcal{I}_h^p(\ddot{e}_I^u, \ddot{e}_I^w)\|e_h^\Sigma\|_{\mathrm{E_f}}\,ds,\end{aligned} \tag{42}$$

where we also use the norm $\|\cdot\|_{\mathrm{E_f}}$ to bound the L^2-norm $\|\cdot\|_{\Omega_f}$. Now, by putting together (37) with (38)–(42) and choosing ϵ_i for $i = 1, \dots, 6$, we obtain

$$\begin{aligned}L_3 &:= \mathcal{M}^p((\dot{e}_h^u, \dot{e}_h^w), (\dot{e}_h^u, \dot{e}_h^w)) + \int_0^t \mathcal{D}^p(\dot{e}_h^w, \dot{e}_h^w)\,ds \\ &\quad + \mathcal{A}_h^p((e_h^u, e_h^w), (e_h^u, e_h^w)) \\ &\quad + \int_0^t \mathcal{M}^f(\dot{e}_h^\Sigma, \dot{e}_h^\Sigma)\,ds + \int_0^t \mathcal{D}^f(\dot{e}_h^\Sigma, \dot{e}_h^\Sigma)\,ds + \mathcal{A}_h^f(e_h^\Sigma, e_h^\Sigma) \\ &\lesssim \int_0^t |||(\dot{e}_I^u, \dot{e}_I^w)|||_{\mathrm{E_p}} \|(e_h^u, e_h^w)\|_{\mathrm{E_p}}\,ds + \int_0^t \mathcal{D}^p(\dot{e}_I^w, \dot{e}_I^w)\,ds \\ &\quad + \mathcal{A}_h^p((e_I^u, e_I^w), (e_I^u, e_I^w)) + \int_0^t \Big(\mathcal{M}^f(\dot{e}_I^\Sigma, \dot{e}_I^\Sigma) + \mathcal{D}^f(\dot{e}_I^\Sigma, \dot{e}_I^\Sigma)\Big)\,ds \\ &\quad + \int_0^t |||\dot{e}_I^\Sigma|||_{\mathrm{E_f}} \|e_h^\Sigma\|_{\mathrm{E_f}}\,ds + \mathcal{A}_h^f(e_I^\Sigma, e_I^\Sigma) \\ &\quad + \int_0^t \mathcal{I}_h^f(\dot{e}_I^\Sigma)\Big(\|\dot{e}_h^u\|_{\Omega_p} + \|\dot{e}_h^w\|_{\Omega_p}\Big)\,ds \\ &\quad + \mathcal{I}_h^p(\dot{e}_I^u, \dot{e}_I^w)\|e_h^\Sigma\|_{\mathrm{E_f}} + \int_0^t \mathcal{I}_h^p(\ddot{e}_I^u, \ddot{e}_I^w)\|e_h^\Sigma\|_{\mathrm{E_f}}\,ds + \mathcal{J}_{\mathcal{B}}^t =: L_4 + \mathcal{J}_{\mathcal{B}}^t.\end{aligned} \tag{43}$$

To bound L_3 from below we reason as for the proof of Therorem 1 to have

$$|L_3| \gtrsim \|(e_h^u, e_h^w)(t)\|_{\mathrm{E}_p}^2 + \|e_h^\Sigma(t)\|_{\mathrm{E_f}}^2.$$

Next, we rearrange the terms for L_4 and write

$$\begin{aligned}L_4 &= \int_0^t |||(\dot{e}_I^u, \dot{e}_I^w)|||_{\mathrm{E_p}} \|(e_h^u, e_h^w)\|_{\mathrm{E_p}}\,ds + \int_0^t |||\dot{e}_I^\Sigma|||_{\mathrm{E_f}} \|e_h^\Sigma\|_{\mathrm{E_f}}\,ds \\ &\quad + \int_0^t \mathcal{I}_h^f(\dot{e}_I^\Sigma)\Big(\|\dot{e}_h^u\|_{\Omega_p} + \|\dot{e}_h^w\|_{\Omega_p}\Big)\,ds + \int_0^t \mathcal{I}_h^p(\ddot{e}_I^u, \ddot{e}_I^w)\|e_h^\Sigma\|_{\mathrm{E_f}}\,ds \\ &\quad + \int_0^t \mathcal{D}^p(\dot{e}_I^w, \dot{e}_I^w)\,ds + \mathcal{A}_h^p((e_I^u, e_I^w), (e_I^u, e_I^w)) \\ &\quad + \int_0^t \Big(\mathcal{M}^f(\dot{e}_I^\Sigma, \dot{e}_I^\Sigma) + \mathcal{D}^f(\dot{e}_I^\Sigma, \dot{e}_I^\Sigma)\Big)\,ds + \mathcal{A}_h^f(e_I^\Sigma, e_I^\Sigma) + \mathcal{I}_h^p(\dot{e}_I^u, \dot{e}_I^w)\|e_h^\Sigma\|_{\mathrm{E_f}}.\end{aligned} \tag{44}$$

We bound all terms by using the definition of the norms, except the last one for which we employ the Young inequality for $\epsilon > 0$

$$\begin{aligned}L_4 &\lesssim \int_0^t \Big(|||(\dot{e}_I^u, \dot{e}_I^w)|||_{\mathrm{E_p}} + |||\dot{e}_I^\Sigma|||_{\mathrm{E_f}} + \mathcal{I}_h^f(\dot{e}_I^\Sigma) \\ &\quad + \mathcal{I}_h^p(\ddot{e}_I^u, \ddot{e}_I^w)\Big)\Big(\|(e_h^u, e_h^w)\|_{\mathrm{E_p}} + \|e_h^\Sigma\|_{\mathrm{E_f}}\Big)\,ds \\ &\quad + \int_0^t \mathcal{D}^p(\dot{e}_I^w, \dot{e}_I^w)\,ds + \mathcal{A}_h^p((e_I^u, e_I^w), (e_I^u, e_I^w)) \\ &\quad + \int_0^t \Big(\mathcal{M}^f(\dot{e}_I^\Sigma, \dot{e}_I^\Sigma) + \mathcal{D}^f(\dot{e}_I^\Sigma, \dot{e}_I^\Sigma)\Big)\,ds \\ &\quad + \mathcal{A}_h^f(e_I^\Sigma, e_I^\Sigma) + \frac{1}{2\epsilon}\mathcal{I}_h^p(\dot{e}_I^u, \dot{e}_I^w)^2 + \frac{\epsilon}{2}\|e_h^\Sigma\|_{\mathrm{E_f}}^2 \\ &\lesssim \int_0^t \Big(|||(\dot{e}_I^u, \dot{e}_I^w)|||_{\mathrm{E_p}} + |||\dot{e}_I^\Sigma|||_{\mathrm{E_f}} + \mathcal{I}_h^f(\dot{e}_I^\Sigma) + \mathcal{I}_h^p(\ddot{e}_I^u, \ddot{e}_I^w)\Big) \\ &\quad \Big(\|(e_h^u, e_h^w)\|_{\mathrm{E_p}} + \|e_h^\Sigma\|_{\mathrm{E_f}}\Big)\,ds \\ &\quad + \int_0^t \Big(|||(\dot{e}_I^u, \dot{e}_I^w)|||_{\mathrm{E_p}}^2 + |||\dot{e}_I^\Sigma|||_{\mathrm{E_f}}^2\Big)\,ds + |||(e_I^u, e_I^w)|||_{\mathrm{E_p}}^2 + |||e_I^\Sigma|||_{\mathrm{E_f}}^2 \\ &\quad + \frac{1}{2\epsilon}\mathcal{I}_h^p(\dot{e}_I^u, \dot{e}_I^w)^2 + \frac{\epsilon}{2}\|e_h^\Sigma\|_{\mathrm{E_f}}^2 =: L_5.\end{aligned} \tag{45}$$

Moreover, we observe that this bound for L_4 is an upper bound also for $L_4 + \mathcal{J}_{\mathcal{B}}^t \lesssim L_5 + \int_0^t \|e_I^r\|_{\Omega_f}^2\,ds$, for sufficiently small ϵ_5, ϵ_6. Finally, we consider ϵ small enough and take the supremum over $(0, t]$ to get

$$\begin{aligned}&\sup_{t\in(0,T]} \|(e_h^u, e_h^w)(t)\|_{\mathrm{E_p}}^2 + \|e_h^\Sigma(t)\|_{\mathrm{E_f}}^2 \\ &\lesssim \int_0^T \mathcal{J}_1(s)\Big(\|(e_h^u, e_h^w)\|_{\mathrm{E_p}} + \|e_h^\Sigma\|_{\mathrm{E_f}}\Big)\,ds + \int_0^T \mathcal{J}_2(s)\,ds + \sup_{t\in(0,T]} \mathcal{J}_3(t) + \int_0^T \|e_I^r\|_{\Omega_f}^2\,ds,\end{aligned}$$

where

$$\mathcal{J}_1 := |||(\dot{\boldsymbol{e}}_I^u, \dot{\boldsymbol{e}}_I^w)|||_{\mathrm{E_p}} + |||\dot{\boldsymbol{e}}_I^\Sigma|||_{\mathrm{E_f}} + \mathcal{I}_h^f(\dot{\boldsymbol{e}}_I^\Sigma) + \mathcal{I}_h^p(\ddot{\boldsymbol{e}}_I^u, \ddot{\boldsymbol{e}}_I^w),$$
$$\mathcal{J}_2 := |||(\dot{\boldsymbol{e}}_I^u, \dot{\boldsymbol{e}}_I^w)|||_{\mathrm{E_p}}^2 + |||\dot{\boldsymbol{e}}_I^\Sigma|||_{\mathrm{E_f}}^2,$$
$$\mathcal{J}_3 := |||(\boldsymbol{e}_I^u, \boldsymbol{e}_I^w)|||_{\mathrm{E_p}}^2 + |||\boldsymbol{e}_I^\Sigma|||_{\mathrm{E_f}}^2 + \mathcal{I}_h^p(\dot{\boldsymbol{e}}_I^u, \dot{\boldsymbol{e}}_I^w)^2.$$

By applying the Gronwall lemma for non-negative functions, cf. [49, Lemma 2.2], we obtain

$$\sup_{t\in(0,T]} \|(\boldsymbol{e}_h^u, \boldsymbol{e}_h^w, \boldsymbol{e}_h^\Sigma)(t)\|_{\mathrm{E}} \lesssim \int_0^T \mathcal{J}_1(s)\,ds + \Big(\int_0^T \mathcal{J}_2(s)\,ds + \sup_{t\in(0,T]} \mathcal{J}_3(t) + \int_0^T \|\boldsymbol{e}_I^r\|_{\Omega_f}^2\,ds\Big)^{\frac{1}{2}}$$

We conclude the proof by using the results in Lemma 4 and estimate the terms $\mathcal{I}_h^f(\cdot)$ and $\mathcal{I}_h^p(\cdot,\cdot)$ by using [29, Lemma 33] as follows

$$\mathcal{I}_h^f(\dot{\boldsymbol{e}}_I^\Sigma)^2 \lesssim \sum_{\kappa\in\mathcal{T}_{h,I}^f} \frac{h_\kappa^{2q_\kappa-2}}{p_{f,\kappa}^{2n-3}} \|\widetilde{\mathcal{E}}\dot{\boldsymbol{\Sigma}}_f\|_{n,\mathcal{K}_\kappa}^2,$$
$$\mathcal{I}_h^p(\dot{\boldsymbol{e}}_I^u, \dot{\boldsymbol{e}}_I^w)^2 \lesssim \sum_{\kappa\in\mathcal{T}_{h,I}^p} \frac{h_\kappa^{2s_\kappa-2}}{p_{p,\kappa}^{2m-3}} \|\widetilde{\mathcal{E}}\dot{\boldsymbol{u}}_p\|_{m,\mathcal{K}_\kappa}^2 + \sum_{\kappa\in\mathcal{T}_{h,I}^p} \frac{h_\kappa^{2r_\kappa-2}}{p_{p,\kappa}^{2\ell-3}} \|\widetilde{\mathcal{E}}\dot{\boldsymbol{w}}_p\|_{\ell,\mathcal{K}_\kappa}^2,$$
$$\mathcal{I}_h^p(\ddot{\boldsymbol{e}}_I^u, \ddot{\boldsymbol{e}}_I^w)^2 \lesssim \sum_{\kappa\in\mathcal{T}_{h,I}^p} \frac{h_\kappa^{2s_\kappa-2}}{p_{p,\kappa}^{2m-3}} \|\widetilde{\mathcal{E}}\ddot{\boldsymbol{u}}_p\|_{m,\mathcal{K}_\kappa}^2 + \sum_{\kappa\in\mathcal{T}_{h,I}^p} \frac{h_\kappa^{2r_\kappa-2}}{p_{p,\kappa}^{2\ell-3}} \|\widetilde{\mathcal{E}}\ddot{\boldsymbol{w}}_p\|_{\ell,\mathcal{K}_\kappa}^2$$

□

We point out that Theorem 3 cannot be used to prove exponential convergence for the *p*-version of the method, as the hidden constant for the bound of the Stein operator depends on the Sobolev index [52].

Remark 1 (Estimates on the fluid velocity and pressure) Approximations for the fluid velocity and pressure can be obtained from the computed stress $\boldsymbol{\Sigma}_{fh}$ according to (5) and $p_f = -d^{-1}\mathrm{tr}(\dot{\boldsymbol{\Sigma}}_f)$, namely one can define

$$\boldsymbol{u}_{fh}(t) = \rho_f^{-1}\nabla_h\cdot\boldsymbol{\Sigma}_f(t) + \int_0^t \boldsymbol{h}_f(s)\,ds + \boldsymbol{u}_{f0}$$
$$\text{and} \quad p_{fh} = -\frac{1}{d}\mathrm{tr}(\dot{\boldsymbol{\Sigma}}_{fh}).$$

Hence, error estimates for these quantities can be derived from Theorem 3 exhibiting the same convergence order with respect to the mesh size and degree of approximation.

4 Time integration

To integrate in time (21) we introduce in $\Omega_p\times(0,T]$ the auxiliary variables $\boldsymbol{v}_{ph} = \dot{\boldsymbol{u}}_{ph}$ and $\boldsymbol{z}_{ph} = \dot{\boldsymbol{w}}_{ph}$ and write the following (modified) formulation: for any $t\in(0,T]$ find $(\boldsymbol{u}_{ph}, \boldsymbol{w}_{ph}, \boldsymbol{v}_{ph}, \boldsymbol{z}_{ph}, \boldsymbol{\Sigma}_{fh}, \boldsymbol{r}_{fh})(t) \in \boldsymbol{W}_h = \boldsymbol{V}_h^p\times\boldsymbol{V}_h^p\times\boldsymbol{V}_h^p\times\boldsymbol{V}_h^p\times\boldsymbol{S}_h^f\times\boldsymbol{\Lambda}_h^f$ s.t.

$$\begin{aligned}(\dot{\boldsymbol{u}}_{ph}-\boldsymbol{v}_{ph},\hat{\boldsymbol{v}})_{\Omega_p} + (\dot{\boldsymbol{w}}_{ph}-\boldsymbol{z}_{ph},\hat{\boldsymbol{z}})_{\Omega_p} + \mathcal{M}^p((\dot{\boldsymbol{v}}_{ph},\dot{\boldsymbol{z}}_{ph}),(\hat{\boldsymbol{u}},\hat{\boldsymbol{w}})) + \mathcal{D}^p(\boldsymbol{z}_{ph},\hat{\boldsymbol{w}})\\ +\mathcal{A}_h^p((\boldsymbol{u}_{ph},\boldsymbol{w}_{ph}),(\hat{\boldsymbol{u}},\hat{\boldsymbol{w}})) + \mathcal{M}^f(\dot{\boldsymbol{\Sigma}}_{fh},\hat{\boldsymbol{\tau}}) + \mathcal{D}^f(\dot{\boldsymbol{\Sigma}}_{fh},\hat{\boldsymbol{\tau}}) + \mathcal{A}_h^f(\boldsymbol{\Sigma}_{fh},\hat{\boldsymbol{\tau}})\\ +\mathcal{B}^f(\boldsymbol{r}_{fh},\hat{\boldsymbol{\tau}}) - \mathcal{B}^f(\hat{\boldsymbol{\lambda}},\dot{\boldsymbol{\Sigma}}_{fh}) + \mathcal{C}^{pf}((\dot{\boldsymbol{u}}_{ph},\dot{\boldsymbol{w}}_{ph}),\hat{\boldsymbol{\tau}})\\ -\mathcal{C}^{fp}(\dot{\boldsymbol{\Sigma}}_{fh},(\hat{\boldsymbol{u}},\hat{\boldsymbol{v}})) = \mathcal{F}(\hat{\boldsymbol{u}},\hat{\boldsymbol{w}},\hat{\boldsymbol{\tau}})\end{aligned}$$

for any $(\hat{\boldsymbol{u}},\hat{\boldsymbol{w}},\hat{\boldsymbol{v}},\hat{\boldsymbol{z}},\hat{\boldsymbol{\tau}},\hat{\boldsymbol{\lambda}})\in\boldsymbol{W}_h$, with initial conditions $\boldsymbol{u}_{ph}(0) = \boldsymbol{u}_{0\,h}, \boldsymbol{v}_{ph}(0) = \boldsymbol{v}_{0\,h}, \boldsymbol{w}_{ph}(0) = \boldsymbol{w}_{0,h}, \boldsymbol{z}_{ph}(0) = \boldsymbol{z}_{0\,h}$ and $\boldsymbol{\Sigma}_{fh}(0) = \boldsymbol{0}$.

By fixing a basis for the spaces $\boldsymbol{V}_h^p$, $\boldsymbol{S}_h^f$, and $\boldsymbol{\Lambda}_h^f$, and denoting by $\boldsymbol{X}(t) = (\boldsymbol{U}_p, \boldsymbol{W}_p, \boldsymbol{V}_p, \boldsymbol{Z}_p, \boldsymbol{S}_f, \boldsymbol{R}_f)^T \in \mathbb{R}^{ndof}$ the vector of the *ndof* expansion coefficients in the chosen basis, the above system can be written equivalently as

$$\begin{bmatrix} I^p & 0 & 0 & 0 & 0 & 0\\ 0 & I^p & 0 & 0 & 0 & 0\\ 0 & 0 & M_\rho^p & M_{\rho_f}^p & -(N_\alpha+L)^T & 0\\ 0 & 0 & M_{\rho_f}^p & M_{\rho_w}^p & -N^T & 0\\ 0 & 0 & 0 & 0 & M^f + D_\delta^f & 0\\ 0 & 0 & 0 & 0 & B^{f\,T} & 0 \end{bmatrix} \begin{bmatrix} \dot{\boldsymbol{U}}_p\\ \dot{\boldsymbol{W}}_p\\ \dot{\boldsymbol{V}}_p\\ \dot{\boldsymbol{Z}}_p\\ \dot{\boldsymbol{S}}_f\\ \dot{\boldsymbol{R}}_f \end{bmatrix}$$
$$+ \begin{bmatrix} 0 & 0 & -I^p & 0 & 0 & 0\\ 0 & 0 & 0 & -I^p & 0 & 0\\ A^e + B_{\beta^2}^p & B_\beta^p & 0 & 0 & 0 & 0\\ B_\beta^p & B^p & 0 & D_{\eta\kappa}^p + D_\gamma^p & 0 & 0\\ 0 & 0 & N_\alpha + L & N & A^f & B^f\\ 0 & 0 & 0 & 0 & 0 & 0 \end{bmatrix} \begin{bmatrix} \boldsymbol{U}_p\\ \boldsymbol{W}_p\\ \boldsymbol{V}_p\\ \boldsymbol{Z}_p\\ \boldsymbol{S}_f\\ \boldsymbol{R}_f \end{bmatrix} = \begin{bmatrix} \boldsymbol{0}\\ \boldsymbol{0}\\ \boldsymbol{F}_p\\ \boldsymbol{G}_p\\ \boldsymbol{H}_f\\ \boldsymbol{0} \end{bmatrix}, \tag{46}$$

with $\boldsymbol{X}(0) = \boldsymbol{X}_0 = (\boldsymbol{U}_0, \boldsymbol{W}_0, \boldsymbol{V}_0, \boldsymbol{Z}_0, \boldsymbol{0}, \boldsymbol{0})^T$. In (46) the block matrices

$$M^p = \begin{bmatrix} M_\rho^p & M_{\rho_f}^p\\ M_{\rho_f}^p & M_{\rho_w}^p \end{bmatrix} \quad \text{and} \quad A^p = \begin{bmatrix} A^e + B_{\beta^2}^p & B_\beta^p\\ B_\beta^p & B^p \end{bmatrix},$$

are the algebraic representation of the bilinear forms $\mathcal{M}^p(\cdot,\cdot)$ and $\mathcal{A}_h^p(\cdot,\cdot)$, respectively. The damping matrix $D_{\eta\kappa}^p + D_\gamma^p$, is associated with $\mathcal{D}^p(\cdot,\cdot)$, while M^f, D_δ^f, A^f, and B^f to $\mathcal{M}^f(\cdot,\cdot), \mathcal{D}^f(\cdot,\cdot), \mathcal{A}_h^f(\cdot,\cdot)$, and $\mathcal{B}^f(\cdot,\cdot)$, respectively. N, N_α, and L are related to the coupling terms in $\mathcal{C}^{fp}(\cdot,\cdot)$. Now, we rewrite problem (46) in a compact form as:

$$\begin{cases} \mathrm{M}\dot{\boldsymbol{X}}(t) + \mathrm{A}\boldsymbol{X}(t) = \boldsymbol{F}(t), \quad t\in(0,T],\\ \boldsymbol{X}(0) = \boldsymbol{X}_0, \end{cases} \tag{47}$$

and partition the interval $[0, T]$ by introducing a time step $\Delta t > 0$ and define the following finite sequence of temporal steps $t^k = k\Delta t$ for $k = 0,\ldots,N_T$, being $N_T = T/\Delta t$. Finally, we integrate system (47) by using a θ-method scheme with $\theta\in[1/2,1]$, cf. [53], and get for $k = 1,\ldots,N_T$

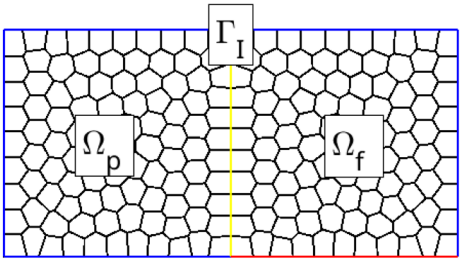

Fig. 1 Test Case 1 and 2: polygonal mesh with Dirichlet (blue), Neumann (red), and interface (yellow) boundaries

Field	Test 1	Test 2
ρ_f, ρ_s	1	1
λ, μ	1,1	1, 0.5
a	1	1
ϕ	0.5	0.5
η/κ	1	1
ρ_w	2	2
β, m	1	1
μ_f	0.5	0.5
α	1	2
δ	1	1
γ	0	0

Fig. 2 Test case 1 and 2. Physical parameters

$$(\mathrm{M}+\Delta t\theta \mathrm{A})\boldsymbol{X}^{k+1}=(\mathrm{M}-\Delta t(1-\theta)\mathrm{A})\boldsymbol{X}^{k}+\Delta t(\theta \boldsymbol{F}^{k+1}+(1-\theta)\boldsymbol{F}^{k}), \tag{48}$$

with $\boldsymbol{X}^k=\boldsymbol{X}(t^k)$.

5 Numerical results

The results obtained in this section have been achieved through the MATLAB code lymph [54]. The verification of the numerical scheme is presented in the first and second tests for which we consider problems (1) and (7) with the following modified coupling conditions on $\Gamma_I\times(0,T]$:

$$\begin{cases}(\alpha\dot{\boldsymbol{u}}_p+\dot{\boldsymbol{w}}_p)\cdot\boldsymbol{n}_p=\boldsymbol{u}_f\cdot\boldsymbol{n}_p-f_I^1,\\ \dot{\boldsymbol{\Sigma}}_f\boldsymbol{n}_p\cdot\boldsymbol{n}_p=\gamma\dot{\boldsymbol{w}}_p\cdot\boldsymbol{n}_p-p_p+f_I^2,\\ \alpha\dot{\boldsymbol{\Sigma}}_f\boldsymbol{n}_p\cdot\boldsymbol{n}_p=\boldsymbol{\sigma}_p\boldsymbol{n}_p\cdot\boldsymbol{n}_p-f_I^3,\\ \dot{\boldsymbol{\Sigma}}_f\boldsymbol{n}_p\wedge\boldsymbol{n}_p=\boldsymbol{\sigma}_p\boldsymbol{n}_p\wedge\boldsymbol{n}_p-f_I^4,\\ \dot{\boldsymbol{\Sigma}}_f\boldsymbol{n}_p\wedge\boldsymbol{n}_p=\delta(\boldsymbol{u}_f-\dot{\boldsymbol{u}}_p)\wedge\boldsymbol{n}_p-f_I^5,\end{cases} \tag{49}$$

with f_I^i, for $i=1,\dots,5$ properly defined to obtain a reference solution. The last example concerns an application of geophysical interest.

5.1 Test case 1

We consider $\Omega=(-1,1)\times(0,1)$ with $\Omega_p=(-1,0)\times(0,1)$ and $\Omega_f=(0,1)\times(0,1)$ such that $\Gamma_I=\{0\}\times(0,1)$, cf. Fig. 1. We fix the final time $T=0.1$, $\Delta t=0.001$, and choose $\theta=\frac{1}{2}$ in (48) (Crank-Nicolson scheme). We select the interface parameters $\alpha=\delta=1$, and $\gamma=0$, set the analytical solution as

$$\boldsymbol{u}_p=\begin{bmatrix}x\frac{t^2}{4}\\ tx^2\frac{y}{2}-y\frac{t^3}{6}\end{bmatrix},\ \boldsymbol{w}_p=\begin{bmatrix}-tx\frac{y^2}{2}+x\frac{t^3}{6}\\ y\frac{t^2}{4}\end{bmatrix},\ \boldsymbol{\Sigma}_f=\begin{bmatrix}\frac{t^3}{6}-t^2\frac{(y^2-x^2)}{4} & 0\\ 0 & -\frac{t^3}{6}-t^2\frac{(y^2-x^2)}{4}\end{bmatrix}, \tag{50}$$

and compute the remaining data accordingly. In particular, in (49) we have $f_I^1=f_I^2=f_I^4=f_5^I=0$ while $f_I^3=-\frac{1}{6}t^3+\frac{3}{4}t^2$. The physical parameters considered are listed in Fig. 2. In Fig. 3 (left), resp. (right), we report the computed error $\|(\boldsymbol{e}^u,\boldsymbol{e}^w)\|_{\mathrm{E_p}}$, resp. $\|\boldsymbol{e}^{\Sigma}\|_{\mathrm{E_f}}$, at the final time $T=0.1$ as a function of the mesh size h_p, resp. h_f, by choosing a polynomial degree equal to 1 and 2. The results agree with the theoretical estimates shown in Theorem 3. In Fig. 4 we plot the computed errors $\|(\boldsymbol{e}^u,\boldsymbol{e}^w)\|_{\mathrm{E_p}}$ and $\|\boldsymbol{e}^{\Sigma}\|_{\mathrm{E_f}}$ at time $T=0.1$ with respect to the polynomial degree $p_p=p_f=1,\dots,5$ for different choices of the the time step: $\Delta t=0.001$ (left) and $\Delta t=0.0001$ (right). As expected, since the analytical solution is polynomial, cf. (50), the error curves decay exponentially until the threshold $\mathcal{O}(\Delta t^2)$, given by the time integration scheme (48), is reached.

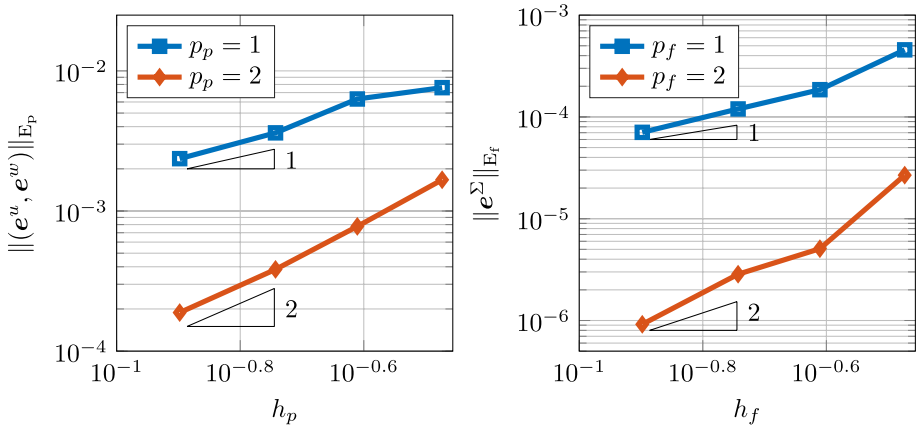

Fig. 3 Test Case 1. Left: log-log plot of the computed error $\|(\boldsymbol{e}^u,\boldsymbol{e}^w)\|_{\mathrm{E_p}}$ as a function of the mesh size h_p for $p_p=1,2$. Right: log-log plot of the computed error $\|\boldsymbol{e}^{\Sigma}\|_{\mathrm{E_f}}$ as a function of the mesh size h_f for $p_f=1,2$. The errors are evaluated at the final time $T=0.1$, with $\Delta t=0.001$

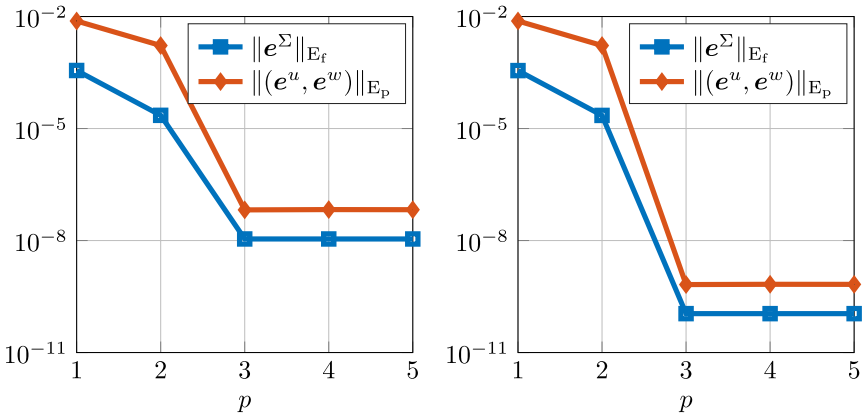

Fig. 4 Test Case 1. Semi-log plot of the computed errors $\|(e^u, e^w)\|_{\mathrm{E_p}}$ and $\|e^{\Sigma}\|_{\mathrm{E_f}}$ as a function of the polynomial degree $p = p_p = p_f$ fixing the number of mesh element equal to 100. The errors are evaluated at the final time $T = 0.1$, with time step $\Delta t = 0.001$ (left), $\Delta t = 0.0001$ (right)

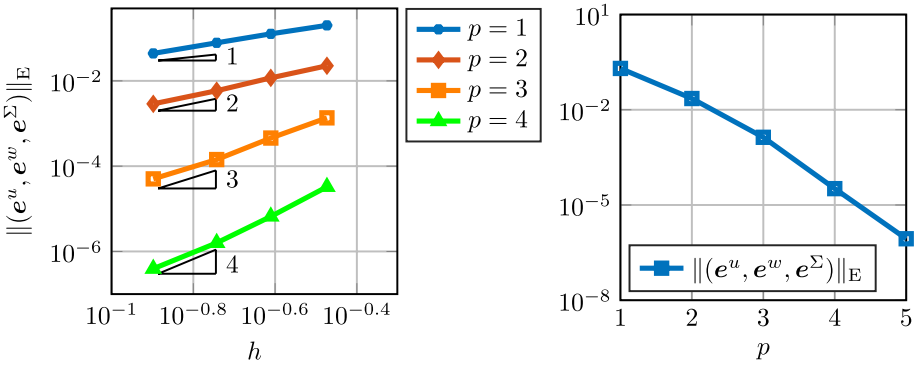

Fig. 5 Test Case 2. Left: log-log plot of the computed error $\|(e^u, e^w, e^{\Sigma})\|_{\mathrm{E}}$ as a function of the mesh size $h = \max(h_p, h_f)$ for $p = p_p = p_f = 1, 2, 3, 4$. Right: semi-log plot of the computed error $\|(e^u, e^w, e^{\Sigma})\|_{\mathrm{E}}$ as a function of the polynomial degree $p = p_p = p_f$ fixing the number of mesh element equal to 100. The errors are evaluated at the final time $T = 0.1$, with $\Delta t = 0.001$

5.2 Test case 2

With the same setup of the previous test case and using the parameters in Table 2, we consider the following analytical solution:

$$\boldsymbol{u}_p = e^{-t}\begin{bmatrix}\sin(x-y)\\ \sin(x-y)\end{bmatrix},\ \boldsymbol{w}_p = -\boldsymbol{u}_p,\ \boldsymbol{\Sigma}_f = (e^{-t}-1)\begin{bmatrix}\cos(x-y) & 0\\ 0 & -\cos(x-y)\end{bmatrix},$$

where $\boldsymbol{\Sigma}^f$ is obtained by selecting

$$\boldsymbol{u}_f = -e^{-t}\begin{bmatrix}\sin(x-y)\\ \sin(x-y)\end{bmatrix},\ \text{and } p_f = 0 \text{ in } \Omega_f.$$

The remaining data are computed accordingly, and in particular, we set $f_I^1 = f_I^4 = f_I^5 = 0$ while $f_I^2 = -e^{-t}\cos(y)$ and $f_I^3 = 3e^{-t}\cos(y)$. We report in Fig. 5 (left) the computed error $\|(e^u, e^w, e^{\Sigma})\|_{\mathrm{E}}$ at time $T = 0.1$, as a function of the mesh size $h = \max(h_p, h_f)$, for a polynomial degree $p = p_p = p_f$ ranging from 1 to 4. The results agree with the theoretical results of Theorem 3. In Fig. 5 the computed error $\|(e^u, e^w, e^{\Sigma})\|_{\mathrm{E}}$ at $T = 0.1$ is shown as a function of the polynomial degree $p = p_p = p_f = 1, \ldots, 5$ fixing the number of mesh element equal to 100. Also in this case the numerical results are aligned with the theoretical estimates in Theorem 3.

5.3 Test case 3

In this last example, we apply our method to a problem similar to the one presented in [18] which is motivated by the coupling of surface and subsurface hydrological systems. On the domain $\Omega = (0, 2) \times (-1, 1)$, we associate the upper half to Ω_f and the lower half to Ω_p. This can be interpreted as a surface flow (lake or river) modeled by the Stokes problem over a poroelastic aquifer, governed by the Biot system. In each subdomain, we consider 800 polygonal elements, see Fig. 6, and polynomial degrees $p_p = p_f = 3$ for a final simulation time $T = 1.5\ s$ and time step $\Delta t = 0.01\ s$. The appropriate interface conditions are enforced along the interface $\Gamma_I = \{y = 0\}$. We consider two cases with different values of η/κ, m, λ_p, and δ, as described in Fig. 7.

The body forces and external source are zero, as well as the initial conditions. The flow is driven by a parabolic fluid velocity imposed on the left boundary of the fluid region. The corresponding boundary conditions are as follows:

$$\begin{cases}
\nabla\cdot\boldsymbol{\Sigma}_f = h(t)(-40y(y-1),0)^T & \text{on } \Gamma_f^{left}\times(0,T],\\
\nabla\cdot\boldsymbol{\Sigma}_f = \boldsymbol{0} & \text{on } \Gamma_f^{top}\times(0,T],\\
\boldsymbol{\Sigma}_f\boldsymbol{n}_f = \boldsymbol{0} & \text{on } \Gamma_f^{right}\times(0,T],\\
p_p = 0 & \text{on } \Gamma_p^{bottom}\times(0,T],\\
\boldsymbol{\sigma}_p\boldsymbol{n}_p = \boldsymbol{0} & \text{on } \Gamma_p^{bottom}\times(0,T],\\
\boldsymbol{u}_p = \boldsymbol{0} & \text{on } \Gamma_p^{left}\cup\Gamma_p^{right}\times(0,T],\\
\boldsymbol{w}_p\cdot\boldsymbol{n}_p = 0 & \text{on } \Gamma_p^{left}\cup\Gamma_p^{right}\times(0,T],
\end{cases}$$

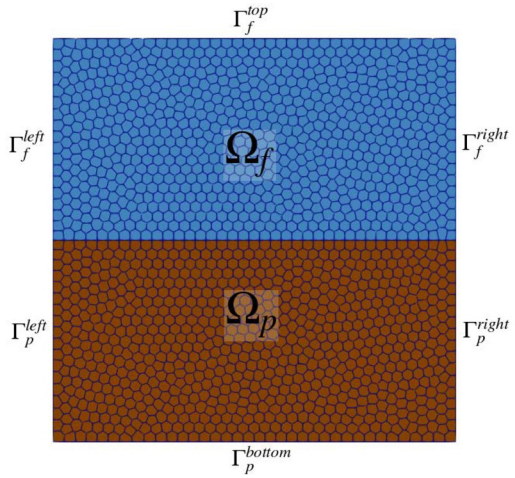

Fig. 6 Test Case 3. Fluid $\Omega_f = (0,2) \times (0,1)$ and poroelastic $\Omega_p = (0,2) \times (-1,0)$ domains. Polygonal mesh with 1600 elements

Field	Set A	Set B
ρ_f, ρ_s	1	1
λ	1	10^6
μ	1	1
a	1	1
ϕ	0.5	0.5
η/κ	1	10^4
ρ_w	2	2
β	1	1
m	1	10^4
μ_f	0.5	0.5
α	1	1
δ	1	100
γ	1	1

Fig. 7 Test case 3. Physical parameters

where $h(t) = 1/(1 + e^{-10(t-1)})$. For each case, we present the plots of computed velocities and pressure at final time T. In particular, in Ω_f we compute $\boldsymbol{u}_f$ using (5) and $p_f = -\frac{1}{2}\mathrm{tr}(\dot{\boldsymbol{\Sigma}}_f)$, while in Ω_p we use (2) to obtain p_p while $\dot{\boldsymbol{u}}_p$ and $\dot{\boldsymbol{w}}_p$ are directly inferred from (48). From the velocity plots, cf. Figs. 8 and 9 (left), we observe that the fluid is driven into the poroelastic medium due to zero pressure at the bottom, which simulates gravity.

The mass conservation $(\alpha\dot{\boldsymbol{u}}_p + \dot{\boldsymbol{w}}_p) \cdot \boldsymbol{n}_p = \boldsymbol{u}_f \cdot \boldsymbol{n}_p$ on the interface with $\boldsymbol{n}_p = (0,1)^T$ indicates continuity of second components of these two velocity vectors, which is observed from the color plot of the velocity, see cf. Figs. 8 and 9 (left). We observe large values for the fluid pressure near the left boundary, which is due to the inflow condition. A discontinuity close to the left lower corner (0, 0) appears due to the mismatch in inflow boundary conditions between the fluid and poroelastic regions. These results are in agreement with [18].

For the set B, the model problem exhibits both locking regimes for poroelasticity: (i) small permeability and storativity and (ii) almost incompressible material as observed in [55]. In particular, the Poisson's ratio $\nu = \frac{\lambda_p}{2(\lambda_p+\nu_p)} = 0.4999995$. The computed solution does not exhibit locking or oscillations. The behavior is qualitatively similar to set A, with larger fluid and poroelastic pressure, see Fig. 9 (right).

6 Conclusions

This study has presented a comprehensive numerical analysis of a polygonal discontinuous Galerkin scheme for simulating fluid exchange between a deformable, saturated poroelastic structure and an adjacent free-flow channel. The investigation specifically addressed wave phenomena governed by the low-frequency Biot model in the poroelastic region and unsteady Stokes flow in the free-flow domain. Transmission conditions enforce conservation laws, achieving coupling at the interface between the two regions and ensuring robust interaction between the subsystems. Spatial

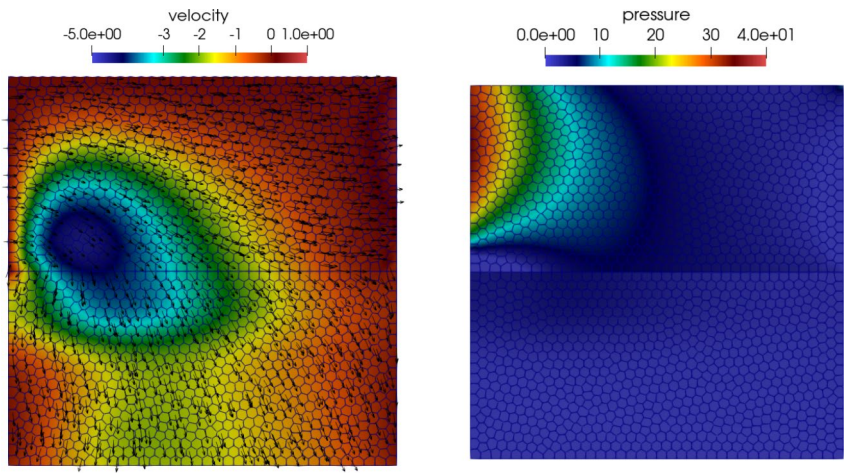

Fig. 8 Test case 3: set A. Computed solutions at final time $T = 1.5$ s. Left: velocities $\boldsymbol{u}_f$ and $\dot{\boldsymbol{u}}_p + \dot{\boldsymbol{w}}_p$ (arrows), $\boldsymbol{u}_{f,2}$ and $\dot{\boldsymbol{u}}_{p,2} + \dot{\boldsymbol{w}}_{p,2}$ (color). Right: computed pressures p_f and p_p

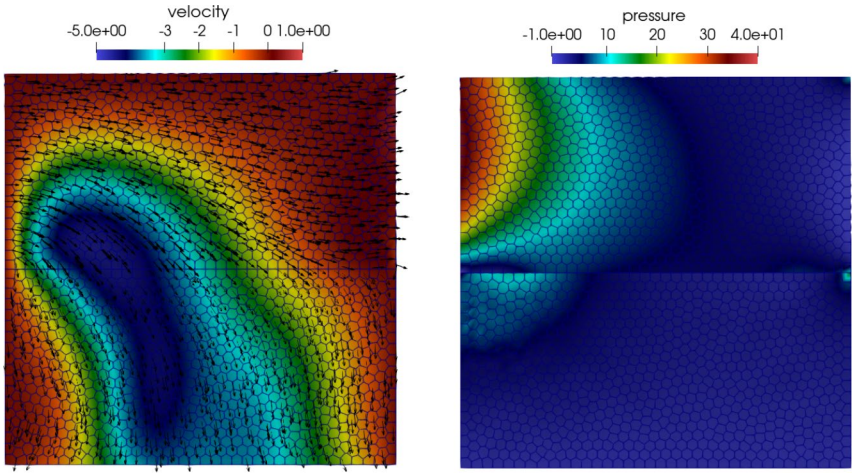

Fig. 9 Test case 3: set B. Computed solutions at final time $T = 1.5\ s$. Left: velocities $\boldsymbol{u}_f$ and $\dot{\boldsymbol{u}}_p + \dot{\boldsymbol{w}}_p$ (arrows), $\boldsymbol{u}_{f,2}$ and $\dot{\boldsymbol{u}}_{p,2} + \dot{\boldsymbol{w}}_{p,2}$ (color). Right: computed pressures p_f and p_p

discretization relied on the two-displacement weak form of the poroelasticity system and a stress-based formulation of the Stokes equation with weakly imposed symmetry. A thorough stability analysis of the proposed semi-discrete formulation was conducted, confirming the robustness of the method. Furthermore, a-priori *hp*-error estimates were derived, providing theoretical guarantees on the accuracy and convergence of the numerical scheme. These findings establish a solid foundation for the reliable and efficient simulation of coupled poroelastic and fluid-flow systems using advanced DG methods as has been shown in the numerical examples.

Appendix A Proof of inf-sup inequality (35)

We first observe that (35) is equivalent to be able to find, for each $\boldsymbol{\lambda}_h \in \boldsymbol{\Lambda}_h^f$ a $\boldsymbol{\tau}_h \in \boldsymbol{S}_h^f$ such that

$$\mathcal{B}^f(\boldsymbol{\lambda}_h, \boldsymbol{\tau}_h) = \|\boldsymbol{\lambda}_h\|_{\Omega_f}^2 \qquad \text{and} \qquad \|\boldsymbol{\tau}_h\|_\star \lesssim \|\boldsymbol{\lambda}_h\|_{\Omega_f}, \tag{51}$$

where

$$\|\boldsymbol{\tau}\|_\star := \|\boldsymbol{\tau}\|_{\mathrm{E}_f} + \sum_{\kappa \in \mathcal{T}_{h,p}^I} p_{p,\kappa} h_\kappa^{-1/2} \|\boldsymbol{\tau}\|_{\partial\kappa \cap \Gamma_I}.$$

We thus construct such a $\boldsymbol{\tau}_h$ by extending the analysis of [44], to include the interface terms of the norm $\|\boldsymbol{\tau}_h\|_\star$. This construction is carried on considering

- the two-dimensional case $\Omega_f \subset \mathbb{R}^2$;
- the fact that our discontinuous space $\boldsymbol{S}_h^f \times \boldsymbol{\Lambda}_h^f$ includes the Amara-Thomas space [56].The extension to the three-dimensional case is not trivial: as indicated in [44], a more complex or completely alternative approach should be considered, and also a different auxiliary finite element space.

This proof relies on the following property, which is verified if we take $\boldsymbol{\Psi} = \boldsymbol{H}^1_{0,\Gamma_I}(\Omega)$, $\boldsymbol{\Psi}_h$ is one of the finite element spaces considered in [44], and $\mathfrak{S}_h^f$ is the tensor space associated to it:

$$\forall \boldsymbol{\tau} \in \boldsymbol{S}^f \quad \exists \boldsymbol{\tau}_h^1 \in \mathfrak{S}_h^f \text{ s.t.} \quad \begin{cases} (\nabla \cdot (\boldsymbol{\tau} - \boldsymbol{\tau}_h^1), \boldsymbol{v}_h)_{\Omega_f} = 0 & \forall \boldsymbol{v}_h \in \boldsymbol{\Psi}_h \subset \boldsymbol{\Psi}, \\ \|\boldsymbol{\tau}_h^1\|_{\boldsymbol{S}^f} \lesssim \|\boldsymbol{\tau}\|_{\boldsymbol{S}^f}, \end{cases} \tag{52}$$

where $\|\boldsymbol{\tau}\|_{\boldsymbol{S}^f}^2 = \|(2\mu_f)^{-1/2}\mathrm{dev}(\boldsymbol{\tau})\|_{\Omega_f}^2 + \|\rho_f^{-1/2}\nabla \cdot \boldsymbol{\tau}\|_{\Omega_f}^2$.

Following the proof of [44, Proposition 2], we introduce a discrete space $\mathfrak{L}_h^f$ approximating $\boldsymbol{\Lambda}^f$ and for a fixed $\boldsymbol{\lambda}_h \in \mathfrak{L}_h^f$ we can build up a continuous tensor $\boldsymbol{\tau} \in \boldsymbol{S}^f$ such that

$$\mathcal{B}^f(\boldsymbol{\lambda}_h, \boldsymbol{\tau}) = \|\boldsymbol{\lambda}_h\|_{\Omega_f}^2 \qquad \text{and} \qquad \|\boldsymbol{\tau}\|_{\boldsymbol{S}^f} \lesssim \|\boldsymbol{\lambda}_h\|_{\Omega_f}. \tag{53}$$

This tensor is defined as $\overline{\boldsymbol{\tau}} = \zeta(\boldsymbol{\psi}) := \begin{bmatrix} -\partial_2\psi_1 & \partial_1\psi_1 \\ \partial_2\psi_2 & \partial_1\psi_2 \end{bmatrix}$, where $\boldsymbol{\psi} \in \boldsymbol{\Psi}$ is the velocity component of the solution to the following Stokes problem:

$$\begin{cases} \mathfrak{a}(\boldsymbol{\psi}, \boldsymbol{\varphi}) + (p, \nabla \cdot \boldsymbol{\varphi})_{\Omega_f} = 0 & \forall \boldsymbol{\varphi} \in \boldsymbol{\Psi}, \\ (q, \nabla \cdot \boldsymbol{\psi})_{\Omega_f} = (\mathfrak{s}(q), \boldsymbol{\lambda}_h)_{\Omega_f} & \forall q \in Q = L^2(\Omega_f), \end{cases}$$

where

$$\mathfrak{s}(q) = \begin{bmatrix} 0 & q \\ -q & 0 \end{bmatrix}, \quad \mathfrak{a}(\boldsymbol{\psi}, \boldsymbol{\varphi}) = (2\mu_f \varepsilon(\boldsymbol{\psi}), \varepsilon(\boldsymbol{\varphi}))_{\Omega_f}.$$

Indeed, $\mathfrak{a}$ is coercive over $\boldsymbol{\Psi}$, $\mathcal{B}^f(\boldsymbol{\lambda}_h, \overline{\boldsymbol{\tau}}) = (\mathfrak{s}(\nabla \cdot \boldsymbol{\psi}), \boldsymbol{\lambda}_h) = \|\nabla \cdot \boldsymbol{\psi}\|_{\Omega_f}^2 = \|\boldsymbol{\lambda}_h\|_{\Omega_f}^2$, and the continuity inequality in (53) follows from $\|\overline{\boldsymbol{\tau}}\|_{\boldsymbol{S}^f}^2 \lesssim \mathfrak{a}(\boldsymbol{\psi}, \boldsymbol{\psi})$ and classical Stokes analysis.

Now, we construct a projection $\Pi_h : \boldsymbol{S}^f \to \mathfrak{S}_h^f$ such that $\overline{\boldsymbol{\tau}}_h = \Pi_h \overline{\boldsymbol{\tau}}$ satisfies (51). Taking a fixed $\boldsymbol{\tau} \in \boldsymbol{S}^f$, we define

$\Pi_h \boldsymbol{\tau} = \boldsymbol{\tau}_h^1 + \boldsymbol{\tau}_h^2$ as a sum of two terms. The first one is the $\boldsymbol{\tau}_h^1$ corresponding to (52). The second one is defined as $\boldsymbol{\tau}_h^2 = \zeta(\boldsymbol{\psi}_h)$, where $\boldsymbol{\psi}_h$ is the solution of the following discrete Stokes problem over an inf-sup stable pair of discrete spaces $\boldsymbol{\Psi}_h \times Q_h \subset \boldsymbol{\Psi} \times Q$:

$$\begin{cases} \mathfrak{a}(\boldsymbol{\psi}_h, \boldsymbol{\varphi}_h) + (p_h, \nabla \cdot \boldsymbol{\varphi}_h)_{\Omega_f} = 0 & \forall \boldsymbol{\varphi}_h \in \boldsymbol{\Psi}_h, \\ (q_h, \nabla \cdot \boldsymbol{\psi}_h)_{\Omega_f} = \mathcal{B}^f(\mathfrak{s}(q_h), \overline{\boldsymbol{\tau}} - \boldsymbol{\tau}_h^1) & \forall q_h \in Q_h. \end{cases} \tag{54}$$

Since $\mathfrak{s}$ is a bijection between Q_h and $\mathfrak{L}_h^f$, we can denote by $\overline{q}_h$ the element of Q_h such that $\mathfrak{s}(\overline{q}_h) = \boldsymbol{\lambda}_h$ and observe that $\mathcal{B}^f(\boldsymbol{\lambda}_h, \boldsymbol{\tau}_h^2) = (\mathfrak{s}(\overline{q}_h), \nabla \cdot \boldsymbol{\psi}_h) = \mathcal{B}^f(\boldsymbol{\lambda}_h, \overline{\boldsymbol{\tau}} - \boldsymbol{\tau}_h^1)$. Moreover, classical Stokes analysis yields $\|\boldsymbol{\tau}_h^2\|_{\boldsymbol{S}^f} \lesssim \|\overline{\boldsymbol{\tau}} - \boldsymbol{\tau}_h^1\|_{\boldsymbol{S}^f}$. Summarizing, we end up with a $\overline{\boldsymbol{\tau}}_h = \boldsymbol{\tau}_h^1 + \boldsymbol{\tau}_h^2$ that satisfies

$$\mathcal{B}^f(\boldsymbol{\lambda}_h, \overline{\boldsymbol{\tau}}_h) = \|\boldsymbol{\lambda}_h\|_{\Omega_f}^2 \qquad \text{and} \qquad \|\overline{\boldsymbol{\tau}}_h\|_{\boldsymbol{S}^f} \lesssim \|\boldsymbol{\lambda}_h\|_{\Omega_f}.$$

Now, $\overline{\boldsymbol{\tau}}_h$ is continuous over Ω_f by construction and $\overline{\boldsymbol{\tau}}_h|_{\Gamma_I} = \mathbf{0}$ because of the zero Dirichlet condition encoded in the spaces $\boldsymbol{\Psi}, \boldsymbol{\Psi}_h$ to which $\boldsymbol{\psi}, \boldsymbol{\psi}_h$ belong, respectively. Therefore $\|\overline{\boldsymbol{\tau}}_h\|_{\boldsymbol{S}^f} = \|\overline{\boldsymbol{\tau}}_h\|_{\mathrm{E_f}}$. Finally, observing that the dG spaces considered in this work are such that $\boldsymbol{S}_h^f \supset \mathfrak{S}_h^f$ and $\boldsymbol{\Lambda}_h = \mathfrak{L}_h^f$, the proof is complete.

□

Acknowledgements IF and IM have been partially supported by ICSC-Centro Nazionale di Ricerca in High Performance Computing, Big Data, and Quantum Computing funded by European Union-NextGenerationEU. The present research is part of the activities of "Dipartimento di Eccellenza 2023–2027". The authors are members of INdAM-GNCS.

Author Contributions All authors contributed equally to this work.

Funding Open access funding provided by Politecnico di Milano within the CRUI-CARE Agreement.

Data Availability No datasets were generated or analysed during the current study.

Declarations

Conflict of interest The authors have no conflict of interest to declare that are relevant to the content of this article.

Open Access This article is licensed under a Creative Commons Attribution 4.0 International License, which permits use, sharing, adaptation, distribution and reproduction in any medium or format, as long as you give appropriate credit to the original author(s) and the source, provide a link to the Creative Commons licence, and indicate if changes were made. The images or other third party material in this article are included in the article's Creative Commons licence, unless indicated otherwise in a credit line to the material. If material is not included in the article's Creative Commons licence and your intended use is not permitted by statutory regulation or exceeds the permitted use, you will need to obtain permission directly from the copyright holder. To view a copy of this licence, visit http://creativecommons.org/licenses/by/4.0/.

References

1. Discacciati M, Miglio E, Quarteroni A (2002) Mathematical and numerical models for coupling surface and groundwater flows. Appl Numer Math 43:57–74
2. Rivière B, Yotov I (2005) Locally conservative coupling of Stokes and Darcy flows. SIAM J Numer Anal 42:1959–1974
3. Ervin VJ, Jenkins EW, Sun S (2009) Coupled generalized nonlinear Stokes flow with flow through a porous medium. SIAM J Numer Anal 47:929–952
4. Gatica G, Meddahi S, Oyarzúa R (2009) A conforming mixed finite-element method for the coupling of fluid flow with porous media flow. IMA J Numer Anal 29:86–108
5. Vassilev D, Wang C, Yotov I (2014) Domain decomposition for coupled Stokes and Darcy flows. Comput Methods Appl Mech Eng 268:264–283
6. Richter T (2017) Fluid-structure interactions: models, analysis and finite elements, vol 118. Springer, Switzerland
7. Mikelić A, Wheeler MF, Wick T (2015) Phase-field modeling of a fluid-driven fracture in a poroelastic medium. Comput Geosci 19:1171–1195
8. Kim J-M (2004) Fully coupled poroelastic governing equations for groundwater flow and solid skeleton deformation in variably saturated true anisotropic porous geologic media. Geosci J 8:291–300
9. Lacis U, Zampogna GA, Bagheri S (2017) A computational continuum model of poroelastic beds. In: Proc. R. Soc. A., vol. 473, p. 20160932
10. Koshiba N, Ando J, Chen X, Hisada T (2006) Multiphysics simulation of blood flow and ldl transport in a porohyperelastic arterial wall model. J Biomech Eng 129(3):374–385
11. Nobile F, Vergara C (2008) An effective fluid-structure interaction formulation for vascular dynamics by generalized Robin conditions. SIAM J Sci Comput 30(2):731–763
12. Showalter RE (2005) Poroelastic filtration coupled to Stokes flow, vol 242. Chapman and Hall/CRC, Boca Raton, pp 229–241
13. Beavers GS, Joseph DD (1967) Boundary conditions at a naturally permeable wall. J Fluid Mech 30(1):197–207
14. Cesmelioglu S (2017) Analysis of the coupled Navier–Stokes/Biot problem. J Math Anal Appl 456:970–993
15. Ambartsumyan I, Ervin VJ, Nguyen T, Yotov I (2019) A nonlinear Stokes–Biot model for the interaction of a non-newtonian fluid with poroelastic media. ESAIM 53(6):1915–1955
16. Bukacč M, Yotov I, Zunino P (2017) Dimensional model reduction for flow through fractures in poroelastic media. ESAIM 51:1429–1471
17. Wen J, He Y (2020) A strongly conservative finite element method for the coupled Stokes–Biot model. Comput Math Appl 80:1421–1442
18. Li T, Yotov I (2022) A mixed elasticity formulation for fluid-poroelastic structure interaction. ESAIM 56(1):1–40
19. Bergkamp EA, Verhoosel CV, Remmers JJC, Smeulders DMJ (2020) A staggered finite element procedure for the coupled Stokes–Biot system with fluid entry resistance. Comput Geosci 24:1497–1522
20. Wilfrid HK (2020) Nonconforming finite element methods for a Stokes/Biot fluid-poroelastic structure interaction model. Results Appl Math 7:100127
21. Bukač M, Yotov I, Zunino P (2015) Partitioning strategies for the interaction of a fluid with a poroelastic material based on a Nitsche's coupling approach. Comput Methods Appl Mech Eng 292:138–170
22. Ambartsumyan I, Khattatov E, Yotov I, Zunino P (2018) A Lagrange multiplier method for a Stokes–Biot fluid-poroelastic structure interaction model. Numer Math 140:513–553

23. Bukač M, Yotov I, Zunino P (2015) An operator splitting approach for the interaction between a fluid and a multilayered poroelastic structure. Numer Methods Part Differ Equ 31:1054–1100
24. Kunwar H, Lee H, Seelman K (2020) Second-order time discretization for a coupled quasi-newtonian fluid-poroelastic system. Int J Numer Methods Fluids 92:687–702
25. Badia S, Quaini A, Quarteroni A (2009) Coupling Biot and Navier-Stokes equations for modelling fluid-poroelastic media interaction. J Comput Phys 228(21):7986–8014
26. Antonietti PF, Botti M, Mazzieri I, Nati Poltri S (2022) A high-order discontinuous Galerkin method for the poro-elasto-acoustic problem on polygonal and polyhedral grids. SIAM J Sci Comput 44(1):1–28
27. Antonietti PF, Botti M, Cancrini A, Mazzieri I (2024) A polytopal discontinuous Galerkin method for the pseudo-stress formulation of the unsteady Stokes problem. https://arxiv.org/abs/2408.08760
28. Antonietti PF, Botti M, Mazzieri I (2024) Discontinuous Galerkin discretization of coupled poroelasticity-elasticity problems. IMA J Numer Anal. https://doi.org/10.1093/imanum/drae093
29. Cangiani A, Dong Z, Georgoulis EH, Houston P (2017) hp[CDATA[hp]]-version Discontinuous Galerkin Methods on Polytopic Meshes. SpringerBriefs in Mathematics. Springer, Switzerland
30. Cangiani A, Dong Z, Georgoulis EH (2017) hp[CDATA[hp]]-version space-time discontinuous Galerkin methods for parabolic problems on prismatic meshes. SIAM J Sci Comput 39(4):1251–1279
31. Antonietti PF, Facciolà C, Russo A, Verani M (2019) Discontinuous Galerkin approximation of flows in fractured porous media on polytopic grids. SIAM J Sci Comput 41(1):109–138
32. Antonietti PF, Verani M, Vergara C, Zonca S (2019) Numerical solution of fluid-structure interaction problems by means of a high order Discontinuous Galerkin method on polygonal grids. Finite Elem Anal Des 159:1–14
33. Antonietti PF, Mazzieri I (2018) High-order discontinuous Galerkin methods for the elastodynamics equation on polygonal and polyhedral meshes. Comput Methods Appl Mech Engrg 342:414–437
34. Antonietti PF, Mazzieri I, Muhr M, Nikolic V, Wohlmuth B (2020) A high-order discontinuous Galerkin method for nonlinear sound waves. J Comput Phys 415:5
35. Antonietti PF, Bonaldi F, Mazzieri I (2020) A high-order discontinuous Galerkin approach to the elasto-acoustic problem. Comput Methods Appl Mech Engrg 358:1–29
36. Antonietti PF, Mazzieri I, Bonaldi F (2020) Simulation of 3D elasto-acoustic wave propagation based on a discontinuous Galerkin spectral element method. Int J Numer Methods Engrg 121:2206–2226
37. Antonietti PF, Botti M, Mazzieri I (2022) On mathematical and numerical modelling of multiphysics wave propagation with polytopal discontinuous Galerkin methods: a review. Vietnam J Math 50(4):997–1028
38. Antonietti PF, Bonetti S, Botti M (2023) Discontinuous Galerkin approximation of the fully coupled thermo-poroelastic problem. SIAM J Sci Comput 45(2):621–645
39. Bonetti S, Botti M, Mazzieri I, Antonietti PF (2023) Numerical modeling of wave propagation phenomena in thermo-poroelastic media via discontinuous Galerkin methods. J Comput Phys 489:112275
40. Corti M, Antonietti PF, Dede' L, Quarteroni AM (2023) Numerical modeling of the brain poromechanics by high-order discontinuous Galerkin methods. Math Models Methods Appl Sci 5:1–33
41. Corti M, Bonizzoni F, Dede' L, Quarteroni AM, Antonietti PF (2023) Discontinuous Galerkin methods for Fisher-Kolmogorov equation with application to α[CDATA[\alpha]]-synuclein spreading in Parkinson's disease. Comput Methods Appl Mech Engrg 417:116450
42. Fumagalli I, Corti M, Parolini N, Antonietti PF (2024) Polytopal discontinuous Galerkin discretization of brain multiphysics flow dynamics. J Comput Phys 513:113115
43. Fumagalli I (2025) Discontinuous Galerkin method for a three-dimensional coupled fluid-poroelastic model with applications to brain fluid mechanics. Eng Math 7(2):130–161
44. Boffi D, Brezzi F, Fortin M (2009) Reduced symmetry elements in linear elasticity. Commun Pure Appl Anal 8(1):95–121
45. Morency C, Tromp J (2008) Spectral-element simulations of wave propagation in porous media. Geophys J Int 175(1):301–345
46. Chiavassa G, Lombard B (2013) Wave propagation across acoustic/Biot's media: a finite-difference method. Commun Comput Phys 13(4):985–1012
47. Arnold D, Lee J (2014) Mixed methods for elastodynamics with weak symmetry. SIAM J Numer Anal 52:2743–2769
48. Lee JJ (2016) Robust error analysis of coupled mixed methods for Biot's consolidation model. J Sci Comput 69:610–632
49. Quarteroni A (2016) Numerical models for differential problems. Springer, Italy
50. Cangiani A, Georgoulis EH, Houston P (2014) hp-version discontinuous Galerkin methods on polygonal and polyhedral meshes. Math Models Methods Appl Sci 24(10):2009–2041
51. Arnold DN, Brezzi F, Cockburn B, Marini LD (2001) Unified analysis of discontinuous Galerkin methods for elliptic problems. SIAM J Numer Anal 39(5):1749–1779
52. Stein EM (1970) Singular integrals and differentiability properties of functions, vol 2. Princeton University Press, Princeton
53. Quarteroni A, Sacco R, Saleri F (2007) Numerical mathematics, vol 2. Springer, Heidelberg
54. Antonietti PF, Bonetti S, Botti M, Corti M, Fumagalli I, Mazzieri I (2025) lymph: Discontinuous polytopal methods for multiphysics differential problems. ACM Trans Math Softw 51:1
55. Yi S-Y (2017) A study of two modes of locking in poroelasticity. SIAM J Numer Anal 55(4):1915–1936
56. Amara M, Thomas J-M (1979) Equilibrium finite elements for the linear elastic problem. Numer Math 33:367–383

Publisher's Note Springer Nature remains neutral with regard to jurisdictional claims in published maps and institutional affiliations.